Title
Peroxy radical behavior during the Transport and Chemical Evolution over the Pacific (TRACE-P) campaign as measured aboard the NASA P-3B aircraft

Journal
Journal of Geophysical Research: Atmospheres, 108(20)

ISSN
0148-0227

Authors
Cantrell, CA
Edwards, GD
Stephens, S
et al.

Publication Date
2003-10-27

DOI
10.1029/2003jd003674

Peroxy radical behavior during the Transport and Chemical Evolution over the Pacific (TRACE-P) campaign as measured aboard the NASA P-3B aircraft

Christopher A. Cantrell,[1] G. D. Edwards,[1] S. Stephens,[1] R. L. Mauldin,[1] M. A. Zondlo,[1,13] E. Kosciuch,[1] F. L. Eisele,[1,2] R. E. Shetter,[1] B. L. Lefer,[1] S. Hall,[1] F. Flocke,[1] A. Weinheimer,[1] A. Fried,[1] E. Apel,[1] Y. Kondo,[3] D. R. Blake,[4] N. J. Blake,[4] I. J. Simpson,[4] A. R. Bandy,[5] D. C. Thornton,[5] B. G. Heikes,[6] H. B. Singh,[7] W. H. Brune,[8] H. Harder,[8,9] M. Martinez,[8,9] D. J. Jacob,[10] M. A. Avery,[11] J. D. Barrick,[11] G. W. Sachse,[11] J. R. Olson,[11] J. H. Crawford,[11] and A. D. Clarke[12]

Received 9 April 2003; revised 24 June 2003; accepted 21 July 2003; published 25 October 2003.

[1] Peroxy radical concentrations were measured aboard the NASA P-3B aircraft during the Transport and Chemical Evolution over the Pacific (TRACE-P) campaign in the spring of 2001 and varied in ways that depended on radical production rates and reactive nitrogen concentrations. Measurements of HO_2, $HO_2 + RO_2$, and OH during this study allowed calculation of radical ratios, examination of functional relationships of these ratios on controlling variables, and comparison with numerical model estimations. Radical production terms show changes in relative contributions at low, middle, and high total production rates that are understandable in terms of systematic variations in the controlling components (trace gas concentrations and photolysis rate coefficients). Ozone tendency calculations indicate net ozone production in the western Pacific basin because the concentrations of critical precursor trace gases (e.g., NO_x, hydrocarbons) are highest there. The dependence of ozone tendency follows the concentration of NO systematically. Peroxy radical levels on the two aircraft ($HO_2 + RO_2$ on the P-3B and HO_2 on the DC-8) during two relatively short prescribed intercomparison periods were in good agreement in one instance and poorer in another given reasonable assumptions about the apportioning of radicals between HO_2 and RO_2. Recommended changes to CH_2O photolysis quantum yields, HO_2 self reaction, and $O(^1D)$ quenching kinetics lead to small changes (<5%) in calculated peroxy radical levels for TRACE-P conditions. There is evidence from this campaign that peroxy radicals are lost by interaction with aerosols and cloud droplets. *INDEX TERMS:* 0317 Atmospheric Composition and Structure: Chemical kinetic and photochemical properties; 0322 Atmospheric Composition and Structure: Constituent sources and sinks; 0365 Atmospheric Composition and Structure: Troposphere—composition and chemistry; 0368 Atmospheric Composition and Structure: Troposphere—constituent transport and chemistry; *KEYWORDS:* photochemistry, peroxy radicals, ozone

Citation: Cantrell, C. A., et al., Peroxy radical behavior during the Transport and Chemical Evolution over the Pacific (TRACE-P) campaign as measured aboard the NASA P-3B aircraft, *J. Geophys. Res.*, *108*(D20), 8797, doi:10.1029/2003JD003674, 2003.

1. Introduction

[2] Observations of free radical concentrations, in conjunction with measurements of controlling variables, are powerful tests of our understanding of the details of tropospheric fast photochemistry [e.g., *Brune et al.*, 1995, 1999; *Cantrell et al.*, 1996, 2003a; *Stevens et al.*, 1997; *Wennberg et al.*, 1998; *Zanis et al.*, 1999; *Faloona et al.*, 2000; *Jaeglé et al.*, 2000; *Burkert et al.*, 2001; *Creasey et*

[1]Atmospheric Chemistry Division, National Center for Atmospheric Research, Boulder, Colorado, USA.
[2]Georgia Institute of Technology, Atlanta, Georgia, USA.
[3]Research Center for Advanced Science & Technology, University of Tokyo, Japan.
[4]University of California, Irvine, Irvine, California, USA.
[5]Drexel University, Philadelphia, Pennsylvania, USA.
[6]University of Rhode Island, Narragansett, Rhode Island, USA.
[7]NASA Ames Research Center, Moffett Field, California, USA.
[8]Pennsylvania State University, University Park, Pennsylvania, USA.
[9]Now at Max Planck Institute for Chemistry, Mainz, Germany.
[10]Harvard University, Cambridge, Massachusetts, USA.
[11]NASA Langley Research Center, Hampton, Virginia, USA.
[12]School of Oceanography and SOEST, University of Hawaii at Manoa, Honolulu, Hawaii, USA.
[13]Now at Southwest Sciences Inc., Santa Fe, New Mexico, USA.

0148-0227/03/2003JD003674

al., 2001; *Davis*, 2001; *Kanaya et al.*, 2001; *Olson et al.*, 2001; *Tan et al.*, 2001; *Sillman et al.*, 2002; *Eisele et al.*, 1996]. In addition to testing the ability of numerical models to predict absolute radical concentrations, we also can examine the functional dependences of radical abundance and ratios upon a number of controlling variables. Studies such as these have met with varied success: sometimes theory and observations agree to within the uncertainties of each [e.g., *Tan et al.*, 2001], while on other occasions unexpectedly large differences are seen that may be partially or entirely unresolved [e.g., *Faloona et al.*, 2000, 2001; *Sillman et al.*, 2002]. The main factors controlling tropospheric free radical abundance for many conditions appear to be well understood, but questions remain regarding their quantitative behavior for high NO_x conditions and in the cold and dry upper troposphere.

[3] The data from the present campaign provide an opportunity to examine tropospheric free radical abundance and chemistry under a range of conditions so that we can continue to test our understanding. This paper presents data collected during the Transport and Chemical Evolution over the Pacific (TRACE-P) campaign, using a relatively new mass spectrometer-based technique that allows quantification of hydroperoxyl radicals (HO_2) and $HO_2 + RO_2$ (RO_2 is the sum of all organic peroxy radicals). These data are combined with other observations and derived quantities (e.g., radical production rates) to quantitatively test understanding of current mechanisms of tropospheric chemistry, including assessment of recent laboratory measurements of potentially critical gas-phase chemical reactions. The chemical evolution of air masses as they are transported across the Pacific basin can then be assessed using photochemical models, if quantitative understanding of photochemical processes has been demonstrated.

2. Peroxy Radical Chemistry

[4] Peroxy radicals are short-lived intermediates that are formed during the oxidation of carbon monoxide (CO), hydrocarbons, and other trace species found in the troposphere. There are a number of processes that form free radicals in the troposphere, including the photolysis of ozone (O_3) in the UV-B spectral region (about 290–350 nm) followed by reaction of the $O(^1D)$ product with water vapor.

$$O_3 + h\nu \rightarrow O(^1D) + O_2 \quad (1)$$

$$O(^1D) + H_2O \rightarrow 2\ OH \quad (2)$$

$$O(^1D) + M \rightarrow O(^3P) + M \quad (3)$$

[5] Ground state oxygen atoms ($O(^3P)$) rapidly combine with oxygen in the troposphere to reform O_3. Photolysis of carbonyl compounds (e.g., formaldehyde, CH_2O, and acetone, $CH_3C(O)CH_3$), peroxides (hydrogen peroxide, H_2O_2, and methylhydroperoxide, CH_3OOH) and other species also produce free radicals. Sometimes the products of these photolysis processes are atoms (e.g., H) and radicals (e.g., HCO, CH_3, CH_3O) that react or combine with molecular oxygen, leading to HO_2 or RO_2 radicals. Radicals are converted to other members of the family (hydroxyl or OH, HO_2, and RO_2) through reaction of OH with various species (CO, CH_2O, O_3, hydrogen, H_2, sulfur dioxide, SO_2, and hydrocarbons), reaction of HO_2 with nitric oxide (NO) and O_3, and reactions of RO_2 with NO. Free radicals are destroyed through formation of peroxides ($HO_2 + HO_2$ reaction and $HO_2 + RO_2$ reaction) and nitrogen compounds ($OH + NO_2$ reaction and $HO_2 + NO_2$ reaction). Products of this chemistry can be deposited or rained out or can lead to reformation of radicals. Radicals are also formed in the oxidation of alkenes and aldehydes by NO_3 radicals that are produced in the reaction of NO_2 with O_3. Reaction of ozone with alkenes leads to formation of OH and peroxy radicals.

[6] When peroxy radicals oxidize NO to NO_2, it results in O_3 formation. Tropospheric free radicals thus are closely coupled with each other, with other important oxidants (O_3 and peroxides), and with reactive nitrogen. Observations of free radicals along with measurements of important controlling species and processes (trace gas levels and photolysis frequencies) provide important (although not necessarily unique) constraints on our understanding of tropospheric photochemistry.

3. Observations and Numerical Modeling

3.1. TRACE-P Aircraft Campaign

[7] The TRACE-P campaign was a two-aircraft (NASA P-3B and DC-8) measurement mission designed (1) to determine the pathways for outflow of chemically and radiatively important gases and aerosols and their precursors from eastern Asia to the western Pacific and (2) to determine the chemical evolution of the Asian outflow over the western Pacific and understand the ensemble of processes that control this evolution [*Jacob et al.*, 1999, 2003]. Flights were conducted from 24 February through 10 April 2001 with flight plans utilizing the respective strengths of each aircraft (P-3B is capable of long boundary layer flight legs and the DC-8 has high altitude ceiling and long range capability). A summary of the campaign can be found in the work of *Jacob et al.* [2003]. The P-3B flew outbound transit flights from Wallops Island, Virginia to Palmdale, California to Kona, Hawaii to Wake Island to Guam to Hong Kong. Local flights were then conducted out of Hong Kong, followed by a transit flight to Yokota Air Base, Japan via Okinawa. Local flights were also deployed from Yokota, followed by return transit flights to Midway Island, a local flight deployed from Midway, with subsequent transit flights to Kona, Palmdale, and Wallops Island. In all, 21 flights consisting of 9 transits and 12 local sorties were conducted. During these flights, air masses from near the surface (150 m AGL) to 7.6 km altitude were sampled. All the flights were conducted during the daytime, approximately centered on local midday, with the exception of the local flight out of Midway Island, which was entirely at night. The DC-8 flew a similar pattern of flights but was capable of sampling at higher altitudes (up to 12 km).

[8] The instruments on the two aircraft included those for in situ observations of free radicals (hydroxyl, OH, HO_2, and RO_2), NO, nitrogen dioxide (NO_2), total odd nitrogen (NO_y), nitric acid (HNO_3), nonmethane hydrocarbons, hal-

ocarbons, alkyl nitrates, oxygenated hydrocarbons, peroxy acetyl nitrate (PAN), CO, carbon dioxide (CO_2), methane (CH_4), SO_2 and other sulfur compounds, O_3, water vapor (H_2O), *j*-values (pseudo-first-order photolysis rate coefficients) for a number of photochemically active species from actinic flux measurements, peroxides (H_2O_2 and organic hydroperoxides), CH_2O, aerosol size distributions, aerosol composition, aerosol optical properties, and some fast measurements that could allow the determination of species fluxes (e.g., O_3). Remote optical measurements of O_3, aerosol scattering and water vapor were also performed.

[9] Since the payload capacity of the P-3B was more limited than the DC-8, it lacked remote sensing capability and the ability to quantify a few important chemical species relevant to free radical chemistry, namely the peroxides, formaldehyde and other oxygenated hydrocarbons (C_2 to C_4 carbonyl compounds, as well as C_1 and C_2 alcohols). Nonmethane hydrocarbon concentrations were measured aboard the P-3B. Under the assumptions that both aircraft flew in similar air masses on average and that the abundance of these unmeasured species (on the P-3B) correlate with CO and longitude (i.e., approximate distance from the Asian source region), species X-to-CO correlations derived from DC-8 data, together with CO observations on the P-3B, were used to estimate species X concentrations aboard the P-3B. While this method may not be totally satisfactory, it does provide concentration estimates that can be used to ascertain an approximate contribution of these species to the free radical budgets for P-3B observing conditions. Figure 1a shows ratios between the two aircraft of 1 km-binned values for several species and demonstrates that on average, the air masses sampled by the two aircraft had similar chemical characteristics (although apparently the P-3B sampled air higher in NO at lower altitudes). The ratios of concentrations are close to unity for many species. Some observed discrepancies are likely due to sampling differences between the two aircraft (due to differences in flight patterns and geographical locations) and possibly also analytical uncertainties.

[10] Sample correlations are shown in Figures 1b and 1c for nine species treated in this fashion for one longitudinal band (four longitudinal bands were used in all). Ratios of compounds of interest to CO were binned by altitude (1 km bins) and longitude (~40 degree bins). The correlations observed on the DC-8 between methanol, ethanol, acetaldehyde, propanal, acetone, and methylethylketone and CO (r^2 values 0.1 to 0.6 for *Apel et al.* [2003] measurements and 0.5 to 0.7 for *Singh et al.* [2003]) and between binned ratios to CO and altitude (r^2 values of 0.3 to 0.95) were fairly good. The correlation between formaldehyde and CO was also good (r^2 = 0.54), but those between the peroxides and

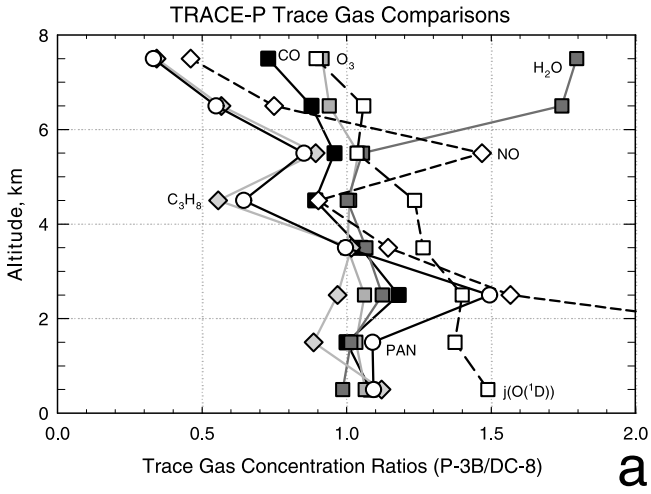

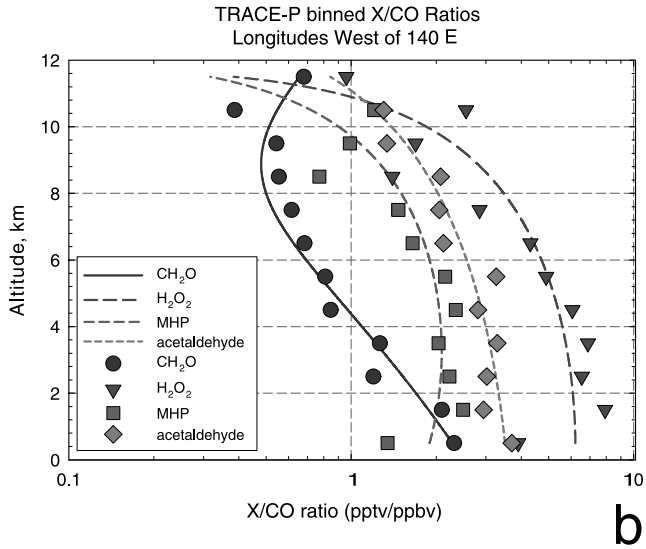

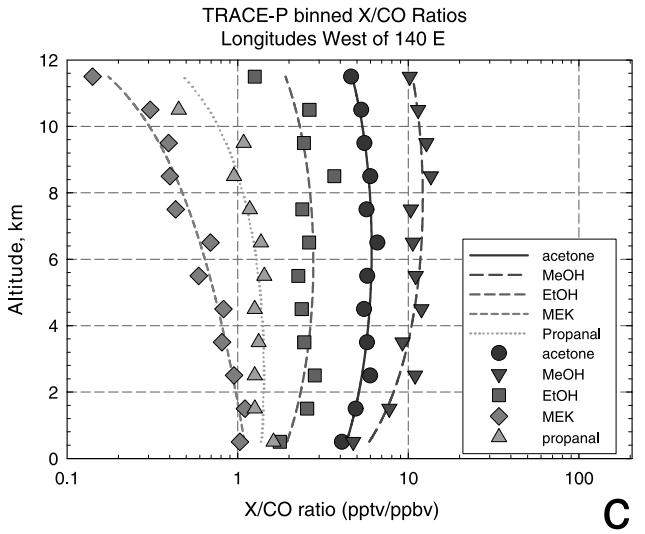

Figure 1. (opposite) (a) Average trace gas concentrations as measured on the P-3B ratioed to those measured on the DC-8 for the TRACE-P campaign, binned into 1-km altitudes (points). Examples of trace gas to carbon monoxide (CO) ratios measured on the DC-8 during TRACE-P binned into 1-km altitudes for (b) formaldehyde (CH_2O), hydrogen peroxide (H_2O_2), methylhydroperoxide (MHP), and acetaldehyde, and for (c) acetone, methanol (MeOH), ethanol (EtOH), and methylethylketone (MEK). Data are separated by longitude. Examples are shown for longitudes west of 140 degrees east. Also shown are second-order polynomials fits (lines) that are used along with CO measurements on the P-3B to estimate concentrations of these species for P-3B observing conditions.

CO were very low (r^2 = 0.01–0.03). Other methods of estimating CH_2O, H_2O_2 and CH_3OOH, such as X-to-H_2O ratios and correlations of concentration with altitude and longitude, were similar. The impacts of using these relationships on the steady state model results are discussed later, but for most conditions using assumed concentrations of these species has little impact (5–10%) on the derived peroxy radical concentrations. Other species (such as NO_x, nonmethane hydrocarbons, and *j*-values) were measured directly aboard the P-3B.

3.2. Measured Peroxy Radical Concentrations

[11] Peroxy radicals were measured by the technique of Peroxy radical Chemical Ionization Mass Spectroscopy (PerCIMS), which has been described in detail elsewhere [*Cantrell et al.*, 2003a; *Edwards et al.*, 2003]. Briefly, ambient peroxy radicals (HO_2 and RO_2) are converted to gas phase sulfuric acid (H_2SO_4) by reaction with NO and SO_2 that are added to the instrument inlet. This reaction scheme involves reaction of HO_2 with NO to form OH, reaction of OH with SO_2 (which forms the $HOSO_2$ adduct), reaction of the $HOSO_2$ adduct with O_2 to form HO_2 and SO_3, and reaction of SO_3 with water vapor. The sulfuric acid product is chemi-ionized by reaction with NO_3^-, and the reagent and product ions are mass filtered and detected. The count rate ratio of HSO_4^- to NO_3^- ions is related to the ambient peroxy radical concentration through calibrations that are conducted on the ground through quantitative photolysis of water vapor at 184.9 nm. Photolysis lamp flux is determined using N_2O chemical actinometry. Two modes of operation are possible, leading to measurement of either [HO_2 + RO_2] or [HO_2], by adjusting the concentrations of NO and SO_2 within the inlet. PerCIMS quantifies $HO_2 + RO_2$ abundance with an estimated uncertainty of 35% (2σ) at levels significantly above the typical detection limit of 10^7 molecules cm^{-3}, and with normal precisions of 10%. Accuracy and precision for HO_2 measurements are 50% (2σ) and 20%, respectively, for levels significantly above the typical detection limit of 2×10^7 molecules cm^{-3}.

[12] Observed values for HO_2 + RO_2 and HO_2 compare well with numerical model estimates (discussed later) of their concentrations, as Figure 2 shows. The small gray points show individual 1-minute average HO_2 + RO_2 concentrations versus model results [*Crawford et al.*, 1999]. Also the observations are grouped into 5-pptv wide concentration bins for three different model scenarios, where the points are the mean concentration of each bin and the error bars show the respective standard deviations. Linear least squares fits to these bin-averaged values yield slopes between 0.83 and 0.92. For the HO_2 observations, the slopes are between 0.97 and 1.01.

[13] Peroxy radical profiles, colored by the total production rate of HO_x and RO_2 radicals (P_{HOx}, defined here as the sum of the rates of radical production from $O(^1D)$ + H_2O, $j(CH_2O)$, $j(H_2O_2)$, $j(CH_3OOH)$, $j(CH_3C(O)CH_3)$, $j(CH_3C(O)CH_2CH_3)$, $j(CH_3CHO)$, and $j(CH_3CH_2CHO)$), are shown in Figure 3a for measured NO_x values less than 100 pptv (for which there is only a small dependence of the radical concentration on NO_x concentration, see Figure 3b). Individual 1-min average values are small colored points. The larger points are 1-km altitude bin averages in the y-direction and 0.05 pptv s^{-1} wide P_{HOx} bins (up to P_{HOx} of 0.3 pptv s^{-1}) with error bars representing the 1-sigma standard deviation of the bin. The observations hint at maxima at middle altitudes (2–5 km) for larger P_{HOx} values; this was seen in the observations during the Tropospheric Ozone about the Spring Equinox (TOPSE) campaign [*Cantrell et al.*, 2003a] and others [e.g., *Tan et al.*, 2001]. HO_2 + RO_2 levels increase with increasing P_{HOx} as expected. There are data at higher P_{HOx} values (up to 1.4 pptv s^{-1}) that are not shown in Figure 3a because there are only a few points in each altitude-P_{HOx} bin.

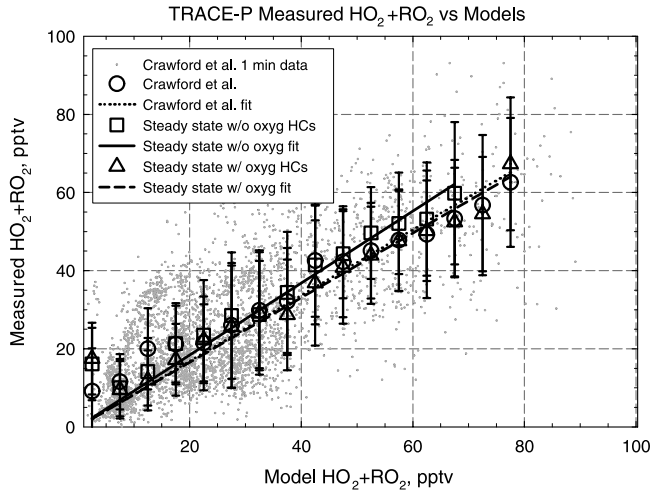

Figure 2. Correlation of observed HO_2 + RO_2 concentrations with modeled concentrations. Small gray symbols are 1-min average concentrations (measurement versus *Crawford et al.* [1999] model), and large symbols are averages for 5 pptv wide bins of modeled results. Three models were used to estimate concentrations: model of Crawford et al., the NCAR steady state model operated without C_2–C_4 carbonyls and C_1–C_2 alcohols, and the NCAR steady state model including the carbonyls and alcohols. Lines are least squares fits to the bin averaged results.

[14] The abundance of HO_2 + RO_2 is also modulated by NO_x. Shown in Figure 3b are the measured bin-averaged (binned by P_{HOx} and NO_x) HO_2 + RO_2 values versus NO_x, colored by P_{HOx} as in Figure 3a. At low NO_x concentrations there is a steady increase in HO_2 + RO_2 mixing ratios with increasing P_{HOx}. As NO_x concentrations increase, $HO_2 + RO_2$ amounts are clearly reduced at a given P_{HOx} due to the increased importance of sink reactions of radicals with NO_x.

[15] Figures 3c and 3d show the same concentration-altitude and concentration-NO_x plots for HO_2 as shown for HO_2 + RO_2 in Figures 3a–3b. There are fewer observations of HO_2, so the statistics are less robust, but the average functional dependencies are similar. Results from the *Crawford et al.* [1999] model for HO_2 + RO_2 are presented in the same manner as the observations in Figures 3e–3f. The solid curves in Figures 3b, 3d, and 3f are discussed in detail later but are the result of fitting the binned observations or model results to a simple equation.

3.3. Modeled Peroxy Radical Concentrations

[16] Three modeled results utilized in the analysis of TRACE-P peroxy radical observations: a point model by

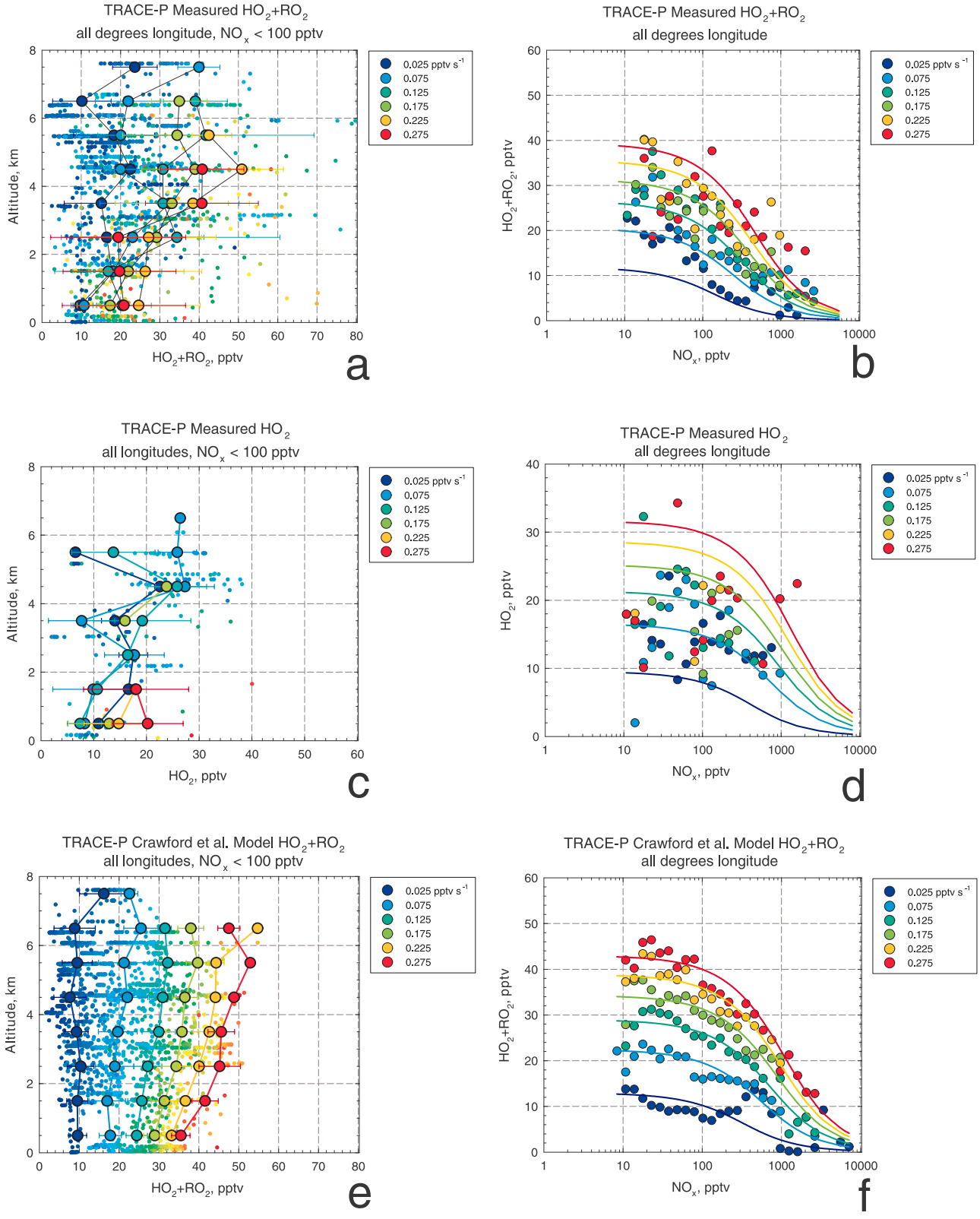

Figure 3. (a) Measured HO_2 + RO_2 concentrations versus altitude colored by P_{HOx} (pptv s^{-1}). Small points are individual 1-min average concentrations, and larger symbols are 1-km altitude bin averages. Data selected for NO_x less than 100 pptv. (b) Observed HO_2 + RO_2 concentrations binned by NO_x concentration and P_{HOx}. Lines are fit to equation (9). (c) Same as Figure 3a for HO_2 observations. (d) Same as Figure 3b for HO_2 observations. (e) Same as Figure 3a using results of *Crawford et al.* [1999] model of TRACE-P observations. (f) Same as Figure 3b using results of *Crawford et al.* [1999] model.

Crawford et al. [1999] applied to TRACE-P data (Figures 3e–3f), and a steady state model from NCAR [*Cantrell et al.*, 1996, 2003b] that was operated without and with estimates of oxygenated hydrocarbon concentrations (C_2–C_4 carbonyls and C_1–C_2 alcohols) determined from correlations with CO and longitude as described earlier; formaldehyde and peroxide estimated concentrations were incorporated in both steady state model runs. Modeled peroxy radical concentrations have estimated uncertainties of 41% (2σ). The model by Crawford et al. was developed for NASA Global Tropospheric Experiment (GTE) missions and is based on a mechanism that describes inorganic and simple hydrocarbon chemistry in detail. Measurements of key species (e.g., NO_x, hydrocarbons, *j*-values) are used as constraints. To avoid problems with initialization, the model is run to diel steady state (i.e., calculations performed over several days with constant constraints but with diurnally varying *j*-values, until sequential days yield the same concentrations). The NCAR steady state model simultaneously solves the time dependent differential rate equations for OH, HO_2, and the various RO_2 radicals assuming that the production and loss of each radical are balanced. The rate terms of the equations are also constrained by observed concentrations of trace gases and measured *j*-values. Here, these models are used as tools to understand the behavior and controlling factors for the peroxy radicals. The references cited give further details about these methods for estimating tropospheric peroxy radical levels. These numerical models do not include estimates of peroxy radical loss on aerosols or cloud droplets. The models also take slightly different approaches in dealing with missing data needed for the calculations (interpolation, previous value, or steady state calculation).

[17] The models agree quite well in their estimates of peroxy radical concentrations as shown in Figure 2. Estimates of HO_2 amounts are nearly identical for all three models, and values for $HO_2 + RO_2$ are very similar for the *Crawford et al.* [1999] model and the NCAR steady state model including higher oxygenated hydrocarbons. The NCAR model without these higher oxygenated species yields $HO_2 + RO_2$ values that are about 10% smaller than the NCAR model runs that include them.

[18] Modeled $HO_2 + RO_2$ and HO_2 values versus altitude are similar to observations. Model radical concentrations versus NO_x are more tightly grouped than the observations, but show some scatter presumably due to factors affecting radical levels that are not accounted for by P_{HOx} and NO_x dependences. There is good agreement between the model results and the measurements as demonstrated by the average $HO_2 + RO_2$ measurement/model ratio of 1.17 ($\sigma = 0.90$) using the *Crawford et al.* [1999] model for all conditions, while the average ratio using the steady-state model (including C_2–C_4 carbonyl compounds and C_1–C_2 alcohols) is 1.04 ($\sigma = 1.18$). This agreement is better than would be expected based on overall measurement uncertainty of individual 1-min samples, partially because random uncertainties are averaged in this process. Subsets of data in which various ranges of NO, CO, nonmethane hydrocarbons, or $HO_2 + RO_2$ were selected lead to measurement/model ratios within 30% of unity, except for a small subset of data with NO concentrations greater than 500 pptv for which the ratios are 2.2 and 3.5 for the steady state and Crawford et al. models, respectively. This apparent underestimation by the models at the very highest NO concentrations does not occur for the highest CO or hydrocarbon concentrations, possibly implying a missing mechanism related to nitrogen oxides (e.g., homogeneous or heterogeneous conversion of products of HO_x–NO_x reactions back into HO_x species), and is similar to observations reported by Brune and coworkers [e.g., *Faloona et al.*, 2000]. A problem with the PerCIMS instrument at high ambient NO concentrations (1000s of pptv) is unlikely since added NO leads to concentrations of several ppmv within the instrument inlet [*Edwards et al.*, 2003]. Measurement/model ratios were also derived for HO_2, with trends similar to those observed for $HO_2 + RO_2$. Measurement/model ratios for two of the models were parsed into a variety of subsets by various trace gas observations and are summarized in Table 1.

Table 1. Ratios of $HO_2 + RO_2$ and HO_2 From PerCIMS Observations to Those Estimated by Two Numerical Models, Parsed Into Subsets by Various Trace Gas Levels

	Crawford et al. [1999] Model		Steady State Model[a]	
Data Subset	Mean	Standard Deviation	Mean	Standard Deviation
	$HO_2 + RO_2$			
All	1.18	0.91	0.97	0.74
NO < 10 pptv	1.29	1.12	1.11	1.06
10 < NO < 100 pptv	1.12	0.67	0.92	0.50
100 < NO < 500 pptv	0.88	0.56	0.68	0.55
NO > 500 pptv	3.52	3.88	2.20	2.65
CO > 200 ppbv	0.82	0.43	0.78	0.47
CO > 500 ppbv	1.27	0.98	0.71	0.18
n-butane > 100 pptv	0.84	0.49	0.71	0.44
n-butane > 300 pptv	0.80	0.33	0.77	0.52
Meas $HO_2 + RO_2 > 10^9 cm^{-3}$	1.28	0.56	1.27	0.65
Model $HO_2 > 5 \times 10^8 cm^{-3}$	0.81	0.28	0.77	0.27
	HO_2			
All	1.21	0.83	1.07	0.52
NO < 10 pptv	0.86	0.53	0.76	0.52
10 < NO < 100 pptv	1.36	0.91	1.13	0.48
100 < NO < 500 pptv	1.51	0.69	1.25	0.49
NO > 500 pptv	–	–	–	–
CO > 200 ppbv	1.33	0.54	1.27	0.38
CO > 500 ppbv	0.87	0.12	0.74	0.09
n-butane > 100 pptv	1.15	0.60	0.98	0.52
n-butane > 300 pptv	1.19	0.51	0.81	0.23
Meas $HO_2 > 8 \times 10^8 cm^{-3}$	2.24	2.11	1.53	0.30
Model $HO_2 > 5 \times 10^8 cm^{-3}$	1.08	0.37	1.17	0.38

[a]NCAR steady state model including estimates of C_2–C_4 carbonyls and C_1–C_2 alcohols. Dash indicates insufficient data in this bin for statistically significant result.

[19] There were three defined measurement periods in which the DC-8 and P-3B flew close to each other in order to compare the observations by similar instruments on both aircraft [*Eisele et al.*, 2003]. The PerCIMS instrument aboard the P-3B obtained $HO_2 + RO_2$ data for two of these periods that can be compared with the chemical conversion/laser induced fluorescence (ATHOS or Atmospheric Total Hydrogen Oxide Sensor) instrument aboard the DC-8 which obtained HO_2 data [*Eisele et al.*, 2003]. This comparison requires some assumptions about the apportioning of peroxy radicals between HO_2 and RO_2 because only $HO_2 + RO_2$ data are available from PerCIMS for these periods. This is done by multiplying the observed $[HO_2 + RO_2]$ by an

assumed or calculated $[HO_2]/[HO_2 + RO_2]$. A constant value for $[RO_2]/[HO_2]$ could be assumed (although this is unrealistic, since the ratio should change in response to changing hydrocarbon concentrations, for example), and in the present case arbitrarily a value of 0.8 (which equates to a $[HO_2]/[HO_2 + RO_2]$ value of 0.56) was employed. The modeling results can also provide estimates of the time dependence of this ratio, which can then be used to obtain HO_2 concentrations from the PerCIMS $HO_2 + RO_2$ values. The model of Crawford et al. yields $[RO_2]/[HO_2]$ radical ratios that vary in space and time from about 0.2 to 1.7 (corresponding to $[HO_2]/[HO_2 + RO_2]$ ratios of 0.83 to 0.37) over the period of the comparisons. The NCAR steady state model (including C_2-C_4 carbonyls and C_1-C_2 alcohols) yields $[RO_2]/[HO_2]$ radical ratios ranging from 0.36 to 2.5 (corresponding to $[HO_2]/[HO_2 + RO_2]$ ratios of 0.74 to 0.28). Using the *Crawford et al.* [1999] model ratios to convert $HO_2 + RO_2$ data to HO_2 yields a mean PerCIMS/ATHOS HO_2 ratio of 1.51 ($1\sigma = 0.66$). Using the steady state model ratios for the conversion yields a mean PerCIMS/ATHOS ratio of 1.30 ($1\sigma = 0.59$), while using a constant $[RO_2]/[HO_2]$ ratio of 0.8 gives a mean PerCIMS/ATHOS ratio of 1.33 ($1\sigma = 0.40$) for these two periods.

[20] The measured and modeled HO_2 values during the three intercomparison periods are shown in Figure 4a, and various ratios of observation and model-estimated HO_2 are shown in Figure 4b. Comparisons of subsets of the data yield good agreement in some cases and poor agreement in others that are summarized in Table 2. While the two measurements and the models agree fairly well on average, there are sometimes systematic and significant differences. Comparison period 1 shows agreement between the models and measurements (except for a few points) well within the range that is expected based on the combined uncertainties (shown by the gray lines in Figure 3b). The models agreed fairly well in period 2, while there are some significant differences that change with time in period 3. The PerCIMS results are consistently greater than the models and ATHOS values during the first part of the flight and consistently less than the models and ATHOS during the latter part. One of the possible reasons for the differences involving the PerCIMS instrument is the fact that all of these comparisons were performed at the very beginning of flights. Our experience has been that the PerCIMS measurements are not always reliable at the very beginning of flights immediately after the instrument has just become operational, probably due to clearing of reagent lines of gases that had remained there for some time and have since become partially oxidized, usually leading to larger apparent peroxy radical concentrations (because inlet NO concentrations are lower). In future comparisons of this type, we recommend that they also be conducted in the middle or near of the end of flights, although we recognize that logistical issues can make this difficult. We are looking at ways to modify the instrument in order to obtain reliable data earlier in flights, and we are involved in ground-based radical comparison studies that will help to further elucidate the behavior of the PerCIMS and ATHOS instruments.

3.4. Photostationary State

[21] The photolysis of NO_2 and the oxidation of NO to NO_2 by ozone and peroxy radicals are sufficiently fast during sunlit periods for the approximation of photochemical steady state for NO to be valid (production and loss of NO in near balance), also called the photostationary state. As reported by several workers in the literature [e.g., *Ridley et al.*, 1992; *Cantrell et al.*, 1997; *Carpenter et al.*, 1998; *Volz-Thomas et al.*, 2003], estimates of peroxy radical concentrations and the $[NO]/[NO_2]$ ratio are possible from the photostationary state approximation.

$$[HO_2 + RO_2]_{PSS} = \frac{k_{NO+O_3}}{k_{NO+HO_2/RO_2}} \left(\frac{j NO_2 [NO_2]}{k_{NO+O_3}[NO]} - [O_3] \right) \quad (4)$$

$$\left(\frac{[NO]}{[NO_2]} \right)_{PSS} = \frac{j NO_2}{k_{NO+HO_2/RO_2}[HO_2 + RO_2] + k_{NO+O_3}[O_3]}, \quad (5)$$

where k_{NO+O_3} is the rate coefficient for reaction of NO with O_3, k_{NO+HO_2/RO_2} is the weighted average rate coefficient for reaction of NO with peroxy radicals, and jNO_2 is the photolysis rate coefficient for NO_2. Observed quantities (on the right-hand side of the equation) are used to calculate $[HO_2 + RO_2]_{PSS}$, and either observed values or steady state $HO_2 + RO_2$ calculated quantities are used to estimate $([NO]/[NO_2])_{PSS}$. Calculations are constrained to jNO_2 greater than 0.003 s^{-1} and are parsed by observed NO concentration. *Cantrell et al.* [1997] point out that PSS estimates of $[HO_2 + RO_2]$ are subject to estimated 60% uncertainties, while PSS $[NO]/[NO_2]$ values have uncertainties around 20%. Photostationary state estimates of $HO_2 + RO_2$ concentrations are about 80% higher than measured for all NO concentrations; PSS values are about 54% higher than observations for NO greater than 10 pptv and average a factor of 2.5 times higher for NO less than 10 pptv for conditions of TRACE-P. Results are similar when comparing with modeled $HO_2 + RO_2$ concentrations. The systematic overestimate of PSS, particularly at low NO levels could be due to an overestimate of $[NO_2]/[NO]$ (i.e., underestimate of $[NO]/[NO_2]$). PSS values of $[NO]/[NO_2]$ are 8 to 12% lower than measured for NO greater than 10 pptv; the PSS ratios average 34% higher than measured for NO less than 10 pptv (i.e., the measured ratios are systematically less than PSS for low NO values). Thus systematic shifts in $[NO]/[NO_2]$ at low NO concentrations could explain at least part of the difference between PSS estimates of $[HO_2 + RO_2]$ and observations during TRACE-P, although the reasons for the PSS and measurements differences are unknown and can only explain part of the differences between observations and PSS estimates of $[HO_2 + RO_2]$. In other studies (e.g., TOPSE, see *Cantrell et al.* [2003b], and BERLIOZ, see *Volz-Thomas et al.* [2003]), differences in PSS and measured $[HO_2 + RO_2]$ values were also seen at lower NO concentrations, but these differences could not be attributed to systematic changes in $[NO]/[NO_2]$. For TRACE-P, there are apparent dependencies of the PSS differences in $[HO_2 + RO_2]$ on altitude, temperature, and water vapor concentration, with higher ratios of PSS $HO_2 + RO_2$ to measured or steady state modeled at higher altitudes, lower water vapor concentrations, and lower temperatures. These could, however, be artifacts of a general anticorrelation between NO and altitude and thus a correlation between NO and water vapor

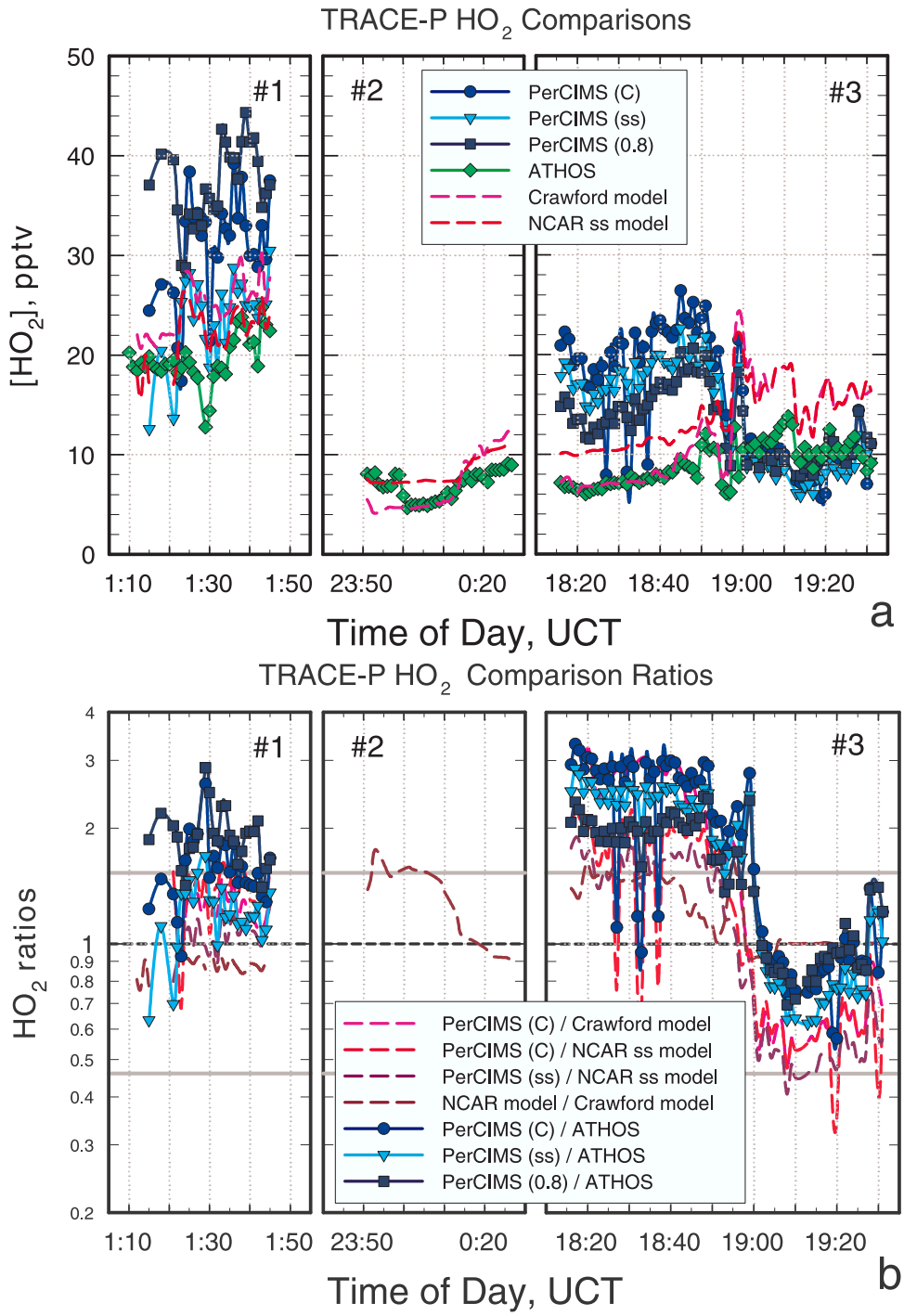

Figure 4. (a) Summary of observed (PerCIMS and ATHOS) and modeled HO_2 concentrations during three comparison periods in which the P-3B and DC-8 aircraft flew in proximity. Comparison 1 was during P-3B flight 8 (DC-8 flight 6), comparison 2 was during P-3B flight 16 (DC-8 flight 14), and comparison 3 was during P-3B flight 23 (DC-8 flight 20). Various assumptions concerning $[HO_2]/[HO_2 + RO_2]$ ratios used to estimate $[HO_2]$ from the PerCIMS $[HO_2 + RO_2]$ data are shown, where C = *Crawford et al.* [1999] model, ss = NCAR steady state model, and 0.8 = a constant ratio. (b) Ratios of observations and models for the three two-aircraft comparison periods. Gray lines show approximate level of expected agreement.

concentration and between NO and temperature. As suggested by other studies, the presence of other oxidants of NO would explain these differences (e.g., halogen oxides, ClO, BrO, IO), but the required abundances (equivalent to 10–20 pptv of BrO at the lowest NO values) appear to be higher than observations or expectations based on current understanding. Another approach is to infer from the PSS differences the rate coefficient between $HO_2 + RO_2$

Table 2. Comparison Between Observation and Numerical Model Estimations of HO_2 Levels During Two (of Three) Periods (IC 1 and IC 3) When the P-3B and DC-8 Flew in Proximity[a]

Instrument or Model IM1	Instrument or Model IM2	Comparison Period	Mean Ratio (IM1/IM2)	Standard Deviation
PerCIMS[b]	ATHOS	IC 1 and IC 3	1.54	0.60
PerCIMS[c]	ATHOS	IC 1 and IC 3	1.29	0.53
PerCIMS[d]	ATHOS	IC 1 and IC 3	1.35	0.41
PerCIMS[b]	ATHOS	IC 1	1.41	0.36
PerCIMS[c]	ATHOS	IC 1	1.06	0.22
PerCIMS[d]	ATHOS	IC 3	1.58	0.66
PerCIMS[c]	ATHOS	IC#3	1.36	0.58
PerCIMS[b]	ATHOS	IC 3 before 18.7	2.05	0.33
PerCIMS[c]	ATHOS	IC 3 before 18.7	1.77	0.28
PerCIMS[b]	ATHOS	IC 3 after 18.9	0.83	0.16
PerCIMS[c]	ATHOS	IC 3 after 18.9	0.70	0.14
PerCIMS[b]	Crawford et al.	IC 1 and IC 3	1.27	0.66
PerCIMS[b]	NCAR steady state	IC 1 and IC 3	1.08	0.40
PerCIMS[c]	NCAR steady state	IC 1 and IC 3	0.89	0.34
NCAR steady state[e]	Crawford et al.	IC 1 and IC 3	1.12	0.25
NCAR steady state	Crawford et al.	IC 1	0.87	0.05
NCAR steady state	Crawford et al.	IC 2	1.44	0.38
NCAR steady state	Crawford et al.	IC 3	1.21	0.24

[a]PerCIMS are observations of $HO_2 + RO_2$ that are converted to HO_2 concentrations by three methods to compare with ATHOS HO_2 observations.
[b]Using $[RO_2]/[HO_2]$ from *Crawford et al.* [1999] model.
[c]Using $[RO_2]/[HO_2]$ from NCAR steady state model.
[d]Using a constant $[RO_2]/[HO_2]$ of 0.8.
[e]NCAR steady state model including estimates of C_2-C_4 carbonyls, and C_1-C_2 alcohols.

and NO that is required to eliminate the differences. On average this inferred rate coefficient agrees with recent recommendations [*Sander et al.*, 2002] but has a much higher temperature coefficient (E/R = 2200 to 3600) and very low preexponential factors (10^{-15} to 10^{-17}). PSS predictions of $HO_2 + RO_2$ concentrations are in good agreement with measurements and steady state model estimates at water vapor mixing ratios greater than about 7000 ppmv. For intermediate water vapor mixing ratios (200 to 7000 ppmv), PSS averages about a factor of 1.9 higher than the observations or model results, and for water vapor mixing ratios less than 200 ppmv, PSS is factors of 3 to 4 higher than the observations or model estimates. These connections between the differences of PSS from observations and model results for $HO_2 + RO_2$ and observed NO, altitude, water vapor, and temperature do not provide direction as to the cause of the differences, since these quantities are somewhat correlated. They do suggest that a temperature dependent laboratory study of the rate coefficient for oxidation of NO by HO_2 and CH_3O_2 (usually the most abundant peroxy radicals) as a function of water vapor concentration would be beneficial to further understanding of the photostationary state in tropospheric photochemistry (although the rate coefficients appear to be well understood in the absence of water vapor).

3.5. Rates of Radical Production and Removal

[22] There have been reports of new laboratory studies of processes relevant to tropospheric peroxy radicals. These include a study of the temperature dependence of HO_2 self-reaction, which could change modeled HO_2 and H_2O_2 abundances. *Christensen et al.* [2002] recommend changes to the bimolecular component (it also has a termolecular channel and a water vapor enhancement factor) of this reaction that reduce the rate coefficient by about a factor of 2 at 230 K (representative of the upper troposphere). The net effect for the P-3B measurement domain during TRACE-P, based on steady state modeling tests, is an average 15% reduction in the overall (bimolecular, termolecular, and water vapor enhancement) rate coefficient (ranging between 4 and 31% reduction) which leads to an average increase in calculated HO_2 of 4.5% (ranging between 0 and 13% increase). This results in an average increase in calculated $HO_2 + RO_2$ of 2.5% (ranging between 1% reduction and 8% increase), whereas calculated H_2O_2 amounts decrease by 8% (1 to 27% range of decrease). Overall the effect of this rate coefficient change is modest for the conditions in which the P-3B flew during TRACE-P.

[23] Recent laboratory-measured quantum yields for formaldehyde photolysis to hydrogen radicals lead to an increase in the importance of this radical source, particularly at lower solar zenith angles [*Smith et al.*, 2002]. Incorporation of these new data into our steady state model leads to very small changes in radical concentrations. For the overall TRACE-P study, the *j*-value for CH_2O leading to radicals is increased by an average of 9.1% ($1\sigma = 2.7\%$), whereas the concentration of HO_2 is only increased by 0.5% ($1\sigma = 0.9\%$). These changes are zenith angle dependent. The *j*-values are larger by an average of 6.4, 8.2, and 16.0% at zenith angles of 10, 40, and 80 degrees, respectively. The HO_2 concentrations change by -0.2, 0.2, and 1.9% for the same zenith angles, respectively. For these calculations, the total $j(CH_2O)$ was kept constant; that is, the molecular channel quantum yields were reduced by the amount by which the radical channel quantum yields were increased.

[24] The quenching rate coefficient for $O(^1D)$ by N_2 has also been recently studied [*Ravishankara et al.*, 2002], leading to recommended rate coefficient values that are 19% ($1\sigma = 0.1\%$) higher for the conditions observed on the P-3B during TRACE-P. This results in radical production rates from reaction of $O(^1D)$ with water vapor that average 11% ($1\sigma = 0.5\%$) smaller. Incorporation of this change into the steady state model leads to peroxy radical levels that average about 3% ($1\sigma = 1.4\%$) lower. If all three recent recommendations [*Smith et al.*, 2002; *Christensen et al.*, 2002; *Ravishankara et al.*, 2002] are incorporated into the model, HO_2 radical levels are decreased by 2.1% while CH_3O_2 and RO_2 amounts are increased about 2.5% for TRACE-P conditions. Total peroxy radical concentrations are nearly unchanged, on average, decreasing by 0.3% ($1\sigma = 2.8\%$). There is an altitude dependence to the changes, with HO_2 averaging a 1% decrease at the surface and a 5% increase at 6 km, and $HO_2 + RO_2$ averaging a 2% decrease and a 2% increase for the surface and 6 km altitude, respectively. These recent laboratory studies, while leading to significant changes in important parameters concerning tropospheric radical chemistry, taken together do not lead to large variations in average calculated peroxy radical levels for the conditions of TRACE-P.

[25] *Thornton et al.* [2002] analyzed data collected from a ground-based site near Nashville and concluded that the rate coefficients for reaction between HO_2 and RO_2 should be

reduced by factors of 3 to 12. Their analysis involves the use of the $NO/NO_2/O_3$ photostationary state to infer RO_2 radical concentrations combined with measurements of HO_2, OH, and a number of other trace gases. Their conclusion that rate coefficients should be reduced is primarily based on a negative correlation between the ratio P'_{HOx}/L_{HOx} (where P'_{HOx} is the radical production rate from O_3 and CH_2O photolysis, which they term primary production, and L_{HOx} is the total radical loss rate, which is mostly due to HO_2 self-reaction and reaction between HO_2 and RO_2) and $F_{HO2+RO2}$ (which is the fraction of radical loss due to reaction between HO_2 and RO_2). In the present study, HO_2 and RO_2 concentrations were estimated from the $HO_2 + RO_2$ observations, with the partitioning determined using steady state modeled $[HO_2]/[HO_2 + RO_2]$. The loss rate of radicals due to reaction of OH with NO_2 was estimated from the steady state model. Thornton et al. limited their analysis to P'_{HOx} greater than 0.5 pptv s^{-1}. However, this condition reduced the number of available data points in the present case to only about 150, such that we allowed data with P'_{HOx} values greater than 0.1 pptv s^{-1}. Although the data are scattered, there is no evidence that P'_{HOx}/L_{HOx} depends in a systematic fashion on $F_{HO2+RO2}$ for TRACE-P; the data are uncorrelated with an r^2 value of 0.02. Even with the uncertainties associated with the PerCIMS observations, a significant change such as that observed by Thornton et al. should be readily discernible. Therefore we see no justification based on this study for recommending changes in rate coefficients for HO_2 plus RO_2 reactions. The apportioning of peroxy radicals (RO_2 versus CH_3O_2 and HO_2) is likely different for TRACE-P (predominantly HO_2 and CH_3O_2) compared with the isoprene-rich environment near Nashville in the summertime (HO_2, CH_3O_2, and a significant fraction of higher RO_2 radicals) and could possibly impact our conclusion. Obviously, the best method for determining rate coefficients is through carefully conducted laboratory studies, but consistency checks with atmospheric observations are extremely useful.

3.6. Loss of Radicals on Aerosols and Clouds

[26] Atmospheric observations and laboratory studies have indicated that peroxy radicals may be removed by reaction on and/or dissolution into aerosols and cloud droplets [*Schwartz*, 1984; *Mozurkewich et al.*, 1987; *Hanson et al.*, 1992; *Cantrell et al.*, 1996; *Saylor*, 1997; *Walcek et al.*, 1997]. The TRACE-P observations covered a wide spectrum of aerosol surface area densities and liquid water abundances that could further test the possibility of multiphase loss of peroxy radicals. Measurement/model ratios of peroxy radical concentrations using either the steady state model or the model of *Crawford et al.* [1999] (neither model includes loss of peroxy radicals on aerosols) were binned based on aerosol surface area density [e.g., *Clarke et al.*, 1996] (converted from measured dry aerosol surface area density using the relationships presented by *Swietlicki et al.* [2000]), and cloud liquid water content. For aerosol surface area densities less than about 100 μm^2-cm^{-3}, the measurement/model ratios are reasonably constant and average about 1.1 and 1.3 using the steady state and Crawford et al. models, respectively. For surface area densities greater than about 100 μm^2-cm^{-3}, measurement/model ratios are lower, averaging 0.78 and 0.84, respectively (Figure 5a); for surface area densities greater than 200 μm^2-cm^{-3}, the ratios are 0.67 and 0.69, respectively. If these changes are interpreted as uptake of radicals onto aerosols and the numerical models are viewed as a way to "standardize" the radical levels, then the measurement/model ratio at higher aerosol loading divided by the measurement/model ratio at lower aerosol loading gives an indication of the effect of aerosols on peroxy radical levels, without relying on absolute model accuracy. These values are 0.70 and 0.65 (using averages greater than 100 μm^2-cm^{-3}), and 0.61 and 0.53 (using averages greater than 200 μm^2-cm^{-3}) using the steady state and Crawford et al. model, respectively. These may be interpreted as a 30–47% loss of peroxy radicals onto aerosols. Applying the above analysis to PerCIMS HO_2 observations does not show a clear trend with aerosol surface area, which may imply that there are either insufficient data to obtain statistically significant conclusions or that the HO_2 observations have enough uncertainty to mask the effect of aerosol uptake. Examination of measurement/model ratios versus altitude indicates that reduction of peroxy radical concentrations relative to the model estimates is greater below 2 km, where aerosol surface area density is greater on average. Peroxy radical losses on aerosols of 40–50% are indicated in the lowest 1 km altitude layer.

[27] Peroxy radical uptake by cloud droplets can be estimated in a fashion similar to that employed for aerosol uptake (Figure 5b). At low liquid water amounts ($<5 \times 10^{-3}$ g m^{-3}), the observations average about 9% larger than the $HO_2 + RO_2$ model levels. For larger liquid water abundances ($>3 \times 10^{-2}$ g m^{-3}), the average measurement/model ratio is 0.66, implying that dense clouds reduce $HO_2 + RO_2$ by about 40% due to radical uptake. Analysis using our HO_2 observations is inconclusive because there are insufficient data to be statistically significant.

[28] The impacts of aerosols and cloud droplets on peroxy radical levels are potentially significant and wide ranging. These effects must be incorporated into models to provide more correct estimates of the total oxidizing capacity of the troposphere. In order to account for these processes properly, models need to account for the details of the uptake including mass accommodation, diffusion, evaporation, and aqueous phase reaction, which can allow calculation of uptake on both aerosols and cloud droplets. The present data can provide a benchmark for these detailed models. Other important effects including the distortion of the photolyzing radiation field can be accounted for through direct observations (as in this study) but must also be accounted for within chemical transport models.

3.7. Calculated P_{HOx} Values

[29] Using observed *j*-values and trace gas concentrations, we are able to calculate the rates of each of the terms of P_{HOx} (all processes which produce HO_x and RO_2) and examine their behavior over the TRACE-P domain. Figure 6a shows the fractional contributions of each of these terms binned by the total P_{HOx} (logarithm scale). Also shown is the average solar zenith angle for each bin (light gray line) as well as white vertical reference lines that divide the plot into three P_{HOx} regions: greater than 0.3, 0.03 to 0.3, and less than 0.03 pptv s^{-1}. At large P_{HOx} (>0.3 pptv s^{-1}), on average more than 80% of P_{HOx} comes

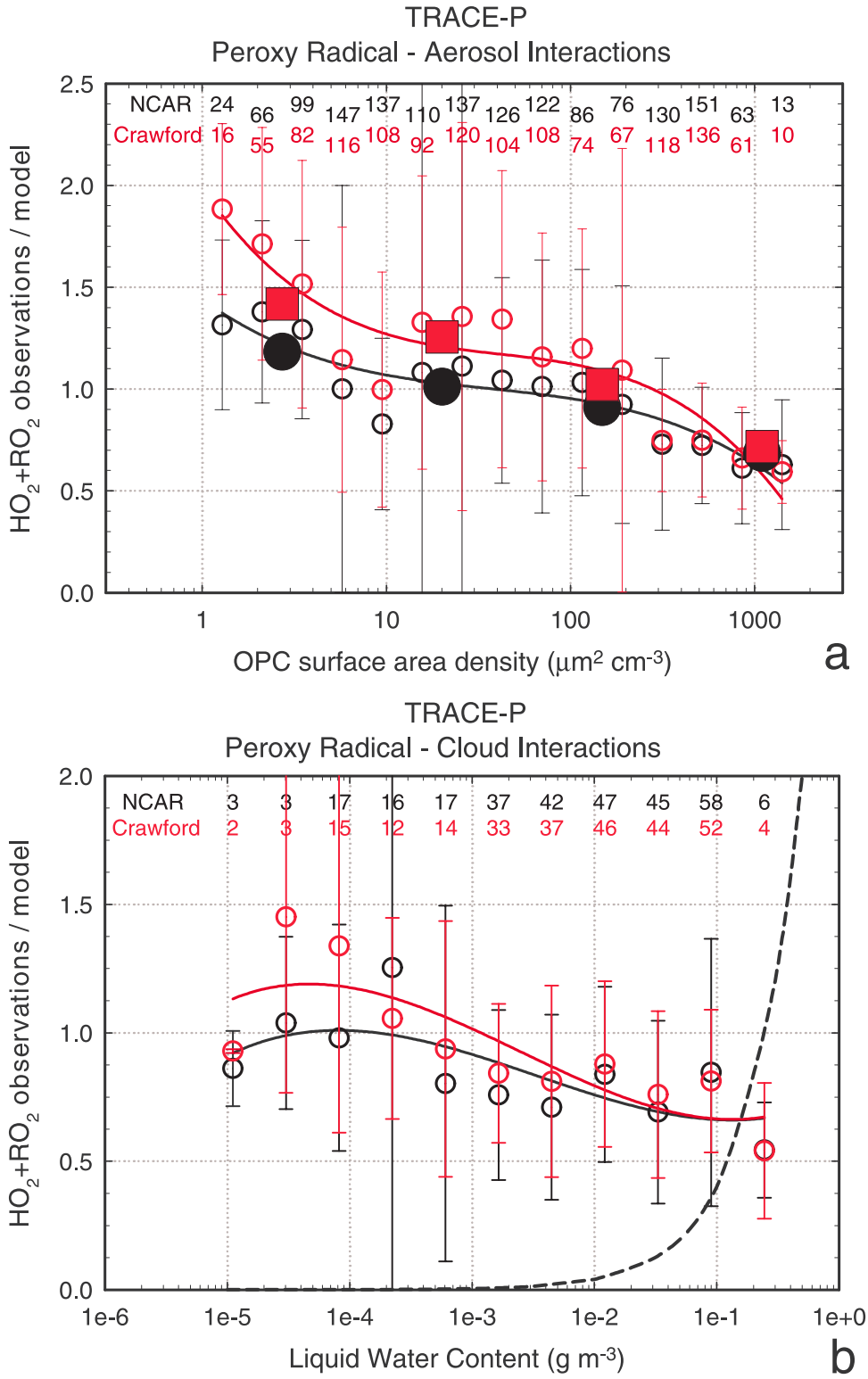

Figure 5. (a) Measurement/model ratios of HO_2 + RO_2 concentrations binned according to ambient aerosol surface area density which was estimated from observed dry aerosol surface area density corrected for hygroscopic growth. Black points utilize the NCAR steady state model (with C_2–C_4 carbonyl and C_1–C_2 alcohol compounds included), and the red points utilize the *Crawford et al.* [1999] model. The small and large points represent fine and coarse bin sizes, respectively, and the lines are polynomial fits to the small points. Numbers at the top of the plot show numbers of data points in each surface area density bin. (b) Same as Figure 5a for cloud liquid water content. Black dashed line shows relative volume of liquid water.

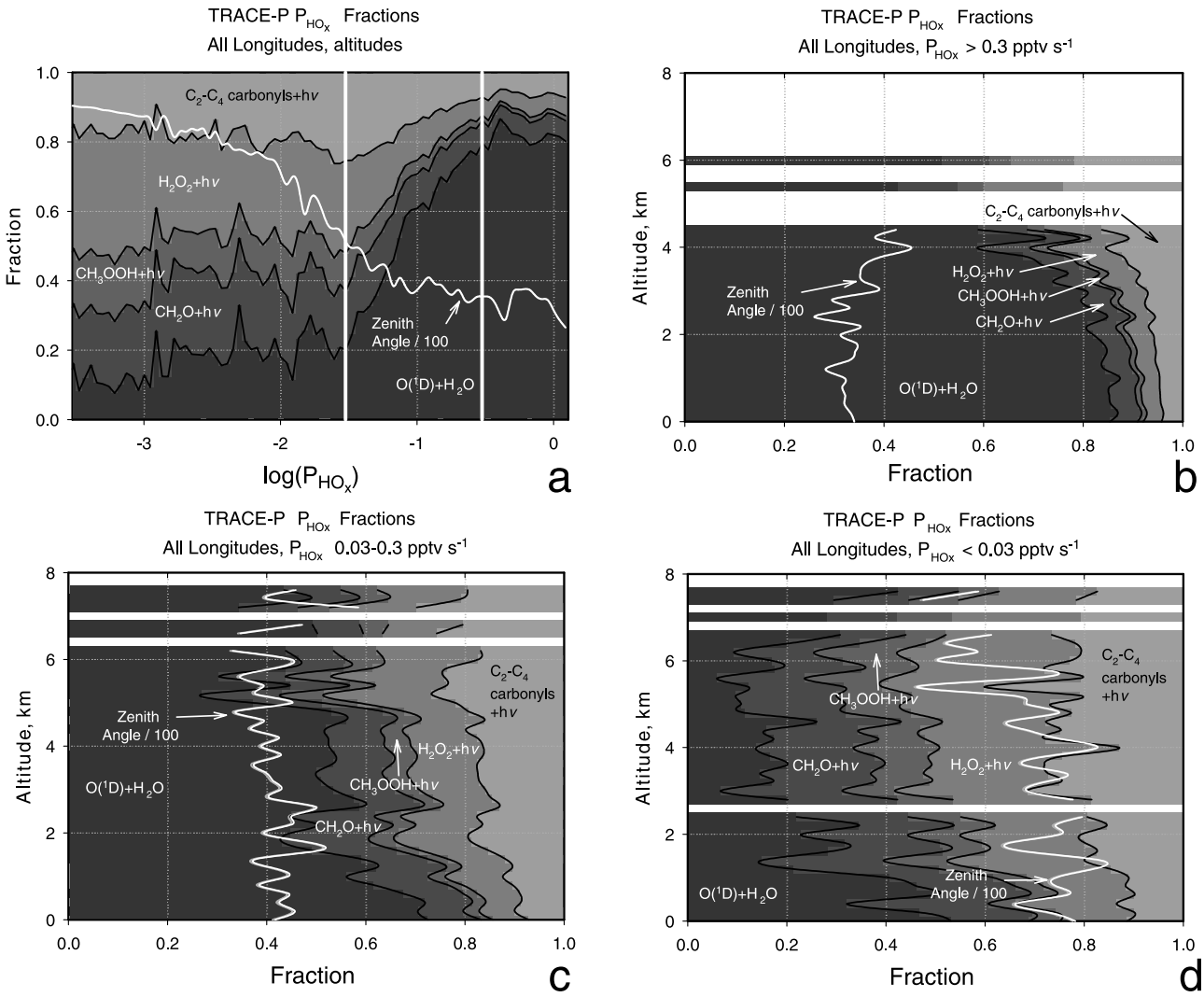

Figure 6. (a) Fractions of P_{HOx} due to five processes (reaction of $O(^1D)$ with water vapor, photolysis of CH_2O, photolysis of CH_3OOH, photolysis of H_2O_2, and photolysis of C_2-C_4 carbonyl compounds) versus bin-averaged P_{HOx}. The average zenith angle for each P_{HOx} bin is also shown (light gray line). White vertical lines separate the plot into three P_{HOx} regions discussed in the text and shown in subsequent plots. (b) Average fractions of P_{HOx} due to five processes versus 0.2-km binned altitude for P_{HOx} values greater than 0.3 pptv s^{-1}. (c) Same as Figure 6b for P_{HOx} between 0.03 and 0.3 pptv s^{-1}. (d) Same as Figure 6b for P_{HOx} less than 0.03 pptv s^{-1}.

from the reaction of $O(^1D)$, produced by ozone photolysis in the UVB, with water vapor. Other photolysis processes produce the remainder of the radicals. These highest average P_{HOx} values correspond with the smallest average solar zenith angles (30–40 degrees). At lower P_{HOx} levels, the relative contribution of $O(^1D)$ plus water vapor systematically decreases, and its average below about 0.03 pptv s^{-1} is 20% or less. This is because these lower average production rates occur in locations sampled by the aircraft where water vapor concentrations are much lower.

[30] At low P_{HOx}, the contribution of $j(H_2O_2)$ to P_{HOx} is about 30%, $j(CH_2O)$ contributes about 20%, $j(CH_3OOH)$ contributes about 10%, and the photolysis of the other oxygenated organics (C_2-C_4 aldehydes and ketones) together makes up about 20%. For an average P_{HOx} value of 0.03 pptv s^{-1}, the average solar zenith angle is about 50 degrees. At lower P_{HOx} values, the zenith angle systematically increases; at an average P_{HOx} of 10^{-3} pptv s^{-1}, the average zenith angle is 87 degrees.

[31] Figures 6b–6d show the altitude dependence of the various P_{HOx} fractions, separated into the three P_{HOx} regimes identified in Figure 6a. The data were placed into 0.2 km altitude bins, and the average solar zenith angle in each bin is also shown. Notice the general decrease in the $O(^1D) + H_2O$ fraction of P_{HOx} with increasing altitude, primarily because of the rapid decrease in H_2O vapor as altitude increases. The change of the relative importance of $O(^1D) + H_2O$ with solar zenith angle is due to the spectral dependence of the photolysis processes. Ozone photolysis occurs at shorter ultraviolet spectral wavelengths, while peroxide and formaldehyde photolyses are more important at longer (but still ultraviolet) wavelengths. This becomes more evident by examining the rates of these processes, rather than simply their fractional contributions. Figures 7a–7c show the bin-

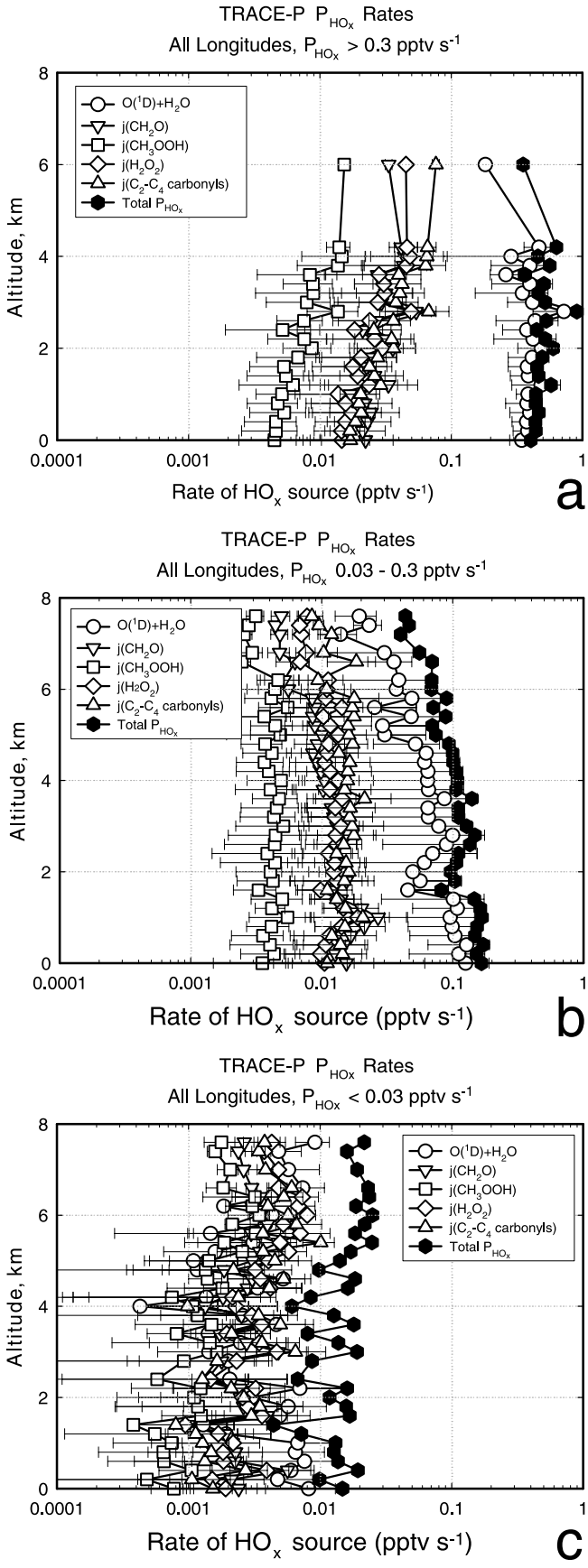

Table 3. Bin-Averaged Components of P_{HOx} From Observations Aboard the P-3B Aircraft From Data Points for Which Peroxy Radical Concentrations Were Calculated Using the NCAR Steady State Model Including C_2-C_4 Carbonyls and C_1-C_2 Alcohols

	P_{HOx} Bin, pptv s^{-1}					
	>0.3		0.03–0.3		<0.03	
Component	0–2 km	4–6 km	0–2 km	4–6 km	0–2 km	4–6 km
P_{HOx}, pptv s^{-1}	0.452	0.504	0.151	0.090	0.012	0.013
O(^{1}D) + H$_2$O, pptv s^{-1}	0.384	0.326	0.107	0.049	0.0049	0.0016
CH$_2$O + hν, pptv s^{-1}	0.024	0.042	0.016	0.009	0.0026	0.0026
H$_2$O$_2$ + hν, pptv s^{-1}	0.017	0.049	0.012	0.011	0.0021	0.0039
CH$_3$OOH + hν, pptv s^{-1}	0.005	0.015	0.004	0.004	0.0007	0.0016
C_2-C_4 carbonyls + hν, pptv s^{-1}	0.022	0.071	0.013	0.017	0.0016	0.0036
j(O(^{1}D)), 10^{-5} s^{-1}	4.52	7.56	1.68	4.71	0.151	0.682
O$_3$, ppbv	39.1	64.0	58.7	52.4	63.0	62.0
H$_2$O, ppmv	19630	5890	9420	1665	5210	670
Q	0.130	0.042	0.065	0.012	0.037	0.005
CO, ppbv	193	265	210	115	221	123
Zenith angle, degrees	32.8	42.0	42.6	38.2	75.0	70.1

averaged rates (and standard deviations) of the processes contributing to P_{HOx} as well as the average of P_{HOx}. Notice that the altitude dependence of the rates of the various processes, as well as P_{HOx}, changes with the P_{HOx} regime. For P_{HOx} greater than 0.3 pptv s^{-1}, O(^{1}D) + H$_2$O and P_{HOx} are nearly independent of altitude, while the other four processes increase with altitude. The middle P_{HOx} regime has O(^{1}D) + H$_2$O decreasing with altitude, and the other four processes (photolysis of CH$_2$O, H$_2$O$_2$, CH$_3$OOH, and C_2-C_4 carbonyls) are almost constant with altitude. In the low P_{HOx} regime, the carbonyl and peroxide photolysis processes increase somewhat with altitude, although there is a reversal of this trend at altitudes greater than about 6 km, which is accompanied by smaller solar zenith angles. This indicates a possible sampling artifact rather than an atmospheric phenomenon.

[32] Can these interesting behaviors be understood by examining the trends of average trace gas mixing ratios and j-values with altitude? Table 3 shows the altitude dependence of factors related to P_{HOx} for various groups of P_{HOx} values. Contributing to the rate of reaction of O(^{1}D) with water are j(O^{1}D), [O$_3$], [H$_2$O], and ambient pressure. All of the binned j-values systematically increase with altitude. The water vapor concentration decreases as altitude increases, while the quenching of O(^{1}D) decreases slightly with altitude, resulting in Q (the fraction of O(^{1}D) reacting with H$_2$O) decreasing with altitude. Ozone concentration increases slightly with altitude. When P_{HOx} is large (>0.3 pptv s^{-1}), the rate of radical production from ozone photolysis followed by reaction of O(^{1}D) with water vapor is nearly independent of altitude up to 6 km as a result of these trends. At intermediate P_{HOx} values (0.03–0.3 pptv s^{-1}), the

Figure 7. (opposite) Altitude dependence of rates of HO_x and RO_2 source reactions and total P_{HOx}, for three P_{HOx} ranges: (a) greater than 0.3 pptv s^{-1}, (b) between 0.03 and 0.3 pptv s^{-1}, and (c) less than 0.03 pptv s^{-1}.

situation is similar, but water concentrations (and Q values) are smaller. Ozone is larger at lower altitudes and smaller at higher altitudes, and the photolysis rate coefficient for ozone to $O(^1D)$ is about 30% smaller, on average, than for the large P_{HOx} group. The net effect is a smaller rate of $O(^1D) + H_2O$ at the surface and a decrease in the rate with altitude. For small P_{HOx} values (<0.03 pptv s^{-1}), water vapor concentrations are even smaller (and somewhat more variable) than the other two P_{HOx} groups, particularly at middle and high altitudes. Ozone is about the same as, and $j(O^1D)$ is less than half that of the middle P_{HOx} group. In the small P_{HOx} group, the contribution of $O(^1D) + H_2O$ increases above about 6 km because $j(O(^1D))$ is larger on average due mostly to sampling at smaller zenith angles. The rate of radical production from $O(^1D) + H_2O$ for the small P_{HOx} group is about 5% that of the intermediate group at the surface and decreases at higher altitudes. These observations are expected and comparable to those observed in other midlatitude measurement campaigns. See Figures 7a–7c and Table 3 for more details of trends in rates of processes that produce HO_x and RO_2 radicals for TRACE-P conditions.

[33] Next we discuss a parameter called the net rate of HO_x and RO_2 formation, which may be useful in assessing the photochemical oxidizing capacity of an air mass, as a complement to other quantities that have been defined in the literature which are related to radical production, namely P_{HOx} (all processes leading to formation of HO_x and RO_2) and $P_{HOx}^{primary}$ (the rates of radical production from $O(^1D) + H_2O$ and the photolysis of C_2-C_4 aldehydes and ketones, which are those production processes not dependent on species produced from radical chemistry). Primary production might also include part of the radicals produced from CH_2O and peroxides, in instances where they were transported from regions of high productivity to areas of lower productivity (such as convective transport of boundary layer air), but this apportioning has not been attempted here. The net rate of HO_x and RO_2 formation is defined as P_{HOx} corrected for those reactions that destroy HO_x and RO_2 in the formation of source species. These reactions are radical-radical reactions that lead to CH_2O, H_2O_2 and CH_3O_2H while consuming HO_2 and RO_2.

$$HO_2 + HO_2 \rightarrow H_2O_2 + O_2 \quad (6)$$

$$HO_2 + CH_3O_2 \rightarrow CH_3O_2H + O_2 \quad (7)$$

$$CH_3O_2 + CH_3O_2 \rightarrow CH_2O + CH_3OH + O_2 \quad (8)$$

[34] Reaction (8) has another channel leading to HO_2 radicals (i.e., does not consume radicals), and it has been reported that reaction (7) has a channel leading to CH_2O [*Elrod et al.*, 2001] which we neglect for this discussion. We designate the net rate of HO_x and RO_2 formation as P_{HOx}^{net}, which is calculated as follows.

$$P_{HOx}^{net} = P_{HOx} - 2\left(k_6[HO_2]^2 + k_7[HO_2][CH_3O_2] + k_8[CH_3O_2]^2\right), \quad (9)$$

where k_6, k_7, and k_8 are the rate constants for reactions (6), (7), and (8), respectively. On first inspection, it might appear that P_{HOx}^{net} and $P_{HOx}^{primary}$ are the same quantities if CH_2O, H_2O_2, and CH_3OOH are in photochemical steady state. However, this is not the case since there are other sources (e.g., reaction of CH_3O_2 with NO to form CH_2O) and sinks (e.g., reactions with OH and other photolysis channels) of these species that do not lead to radical production or loss.

[35] A well-defined relationship between $(HO_2 + RO_2)$/sqrt(P_{HOx}) and NO_x might be expected, since it has been shown that $HO_2 + RO_2$ has a clear relationship with NO_x for a given P_{HOx} level (Figure 3), and that at a given NO_x level, the radical concentration depends approximately on the square root of P_{HOx}. Figure 8a shows $HO_2 + RO_2$ observations divided by the square root of the three P_{HOx} ratios (total, net and primary) versus the binned observed NO_x concentration (log scale). Each of the correlations is excellent, with r^2 correlation coefficients of 0.98, 0.96, and 0.93 for ratios utilizing net, total, and primary production, respectively. The negative slopes are consistent with the results presented in Figure 3, in which the $HO_2 + RO_2$ concentration is lower for a given P_{HOx} as NO_x increases. Treatment of model radical concentrations in the same fashion yields very similar results.

[36] Bin averaged P_{HOx}^{net}/P_{HOx} ratios versus NO_x concentration are shown in Figure 8b. Also shown are P_{HOx} and total peroxide concentrations in the same NO_x bins. At NO_x concentrations less than about 200 pptv, P_{HOx}^{net} is 20 to 30% of P_{HOx} because radical concentrations tend to be higher, and thus peroxide production rates are also larger. For NO_x concentrations greater than about 2000 pptv, P_{HOx}^{net}, and P_{HOx} are nearly equal, due to low radical concentrations and small rates of radical production. P_{HOx} and total peroxide concentrations are larger for the lower concentration NO_x bins, and are smaller for higher NO_x concentrations. Also shown in Figure 8b are the $P_{HOx}^{primary}/P_{HOx}$ ratios for comparison. Note that this ratio gradually decreases as NO_x increases but there is no sudden change as in the case of the P_{HOx}^{net}/P_{HOx} ratios.

[37] We can isolate the HO_x and RO_2 gross production and loss for each of the three reservoir species (CH_2O, H_2O_2, and CH_3OOH), and calculate a net production of radicals for each. These calculated values are shown in Figure 8c, in which net radical production rates (radical production minus loss) for each species versus the gross production of radicals from photolysis of the corresponding reservoir species are shown. Since the rate of reaction (8) is small, production of formaldehyde results in net radical formation, while production of peroxides yields net radical destruction, even without accounting for possible heterogeneous processes which would lead to even larger net radical loss. The slopes of these correlations allow estimation of the number of radicals destroyed per radical produced from these three species (net radical destruction efficiency). The number of radicals lost per radical produced is 0.04 for CH_2O, 2.5 for H_2O_2, and 8.5 for CH_3O_2H. Clearly, there is variability in the efficiencies of radicals produced from these reservoirs, but these quantities provide average values for the conditions of TRACE-P.

4. Functional Relationships

4.1. $HO_2 + RO_2$ and HO_2 Dependence on NO_x and P_{HOx}

[38] The behavior of $HO_2 + RO_2$ versus NO_x and P_{HOx} can be adequately explained by a simple function in which

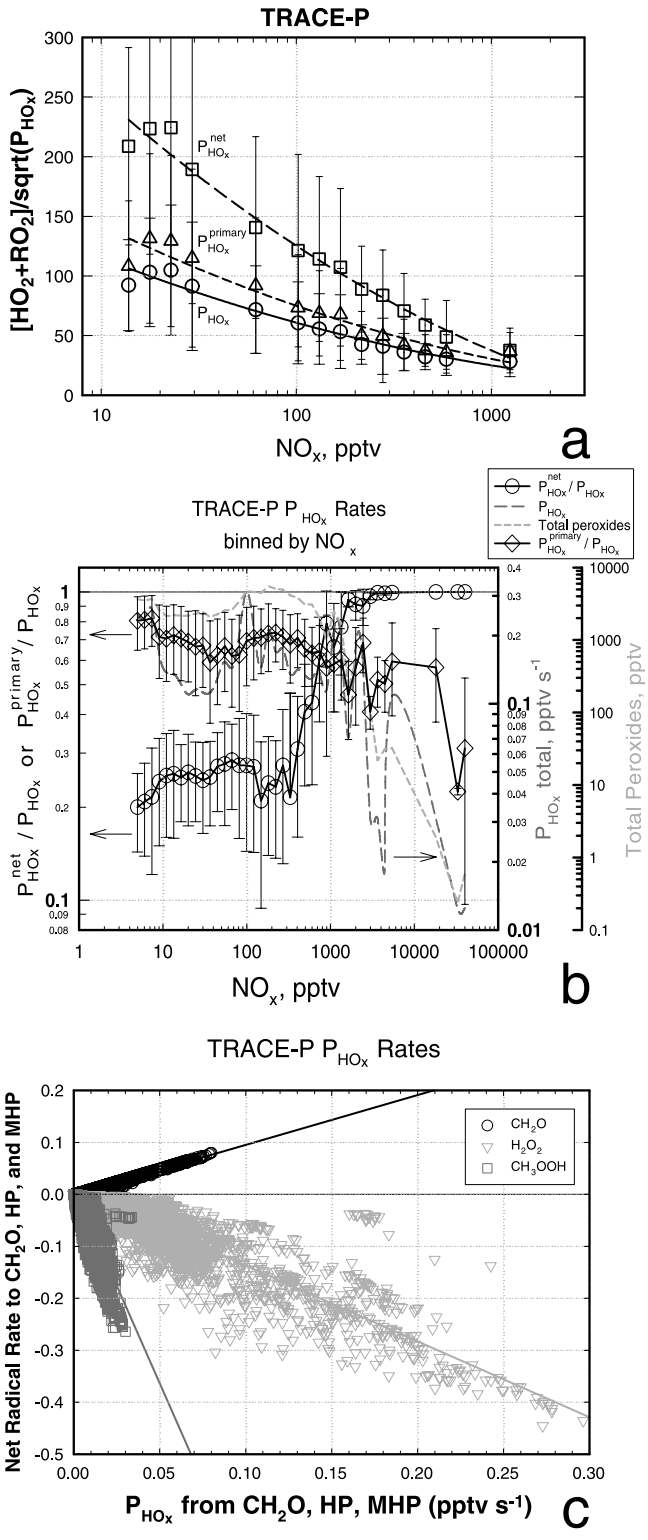

Figure 8. (a) Ratios of measured $HO_2 + RO_2$ to the square root of three values of P_{HOx} versus binned measured NO_x. (b) Mean ratios of P^{net}_{HOx} (circles) and $P^{primary}_{HOx}$ (diamonds) to total P_{HOx} versus binned NO_x. Also shown is total P_{HOx} (dark gray line) and total peroxide concentrations (light gray line) (secondary axes on right). (c) Net rate of radical production from formation and reactions of CH_2O (black), H_2O_2 (light gray) and CH_3OOH (dark gray).

P_{HOx} is assumed equal to the sum of two loss processes, one dependent on the square of the $HO_2 + RO_2$ concentration (a surrogate for HO_2 self-reaction and reaction between HO_2 and RO_2), and one dependent on the product of the concentrations of $HO_2 + RO_2$ and NO_x (a surrogate for OH + NO_2 and other HO_x-NO_x reactions).

$$P_{HOx} = k_{RR}[HO_2 + RO_2]^2 + k_{RN}[HO_2 + RO_2][NO_x], \quad (10)$$

where k_{RR} and k_{RN} refer to the effective rate coefficients for radical-radical and radical-NO_x reactions, which are fit parameters. It is possible that other forms of equation (10) might do an equal or better job of fitting the observations (e.g., an exponential power greater than unity on $[NO_x]$ to account that loss of HO_x by reaction with NO_x is mostly dependent on OH), but the present equation performs satisfactorily and is based on an understanding of the radical loss mechanisms. The solution of equation (10) leads to the following relation between $[HO_2 + RO_2]$, P_{HOx} and $[NO_x]$.

$$[HO_2 + RO_2] = \sqrt{A + B^2} - B$$
$$\text{where, } A = \frac{P_{HOx}}{k_{RR}} \text{ and } B = \frac{k_{RN}[NO_x]}{2\,k_{RR}} \quad (11)$$

[39] One can see that when B is small relative to A (i.e., $[NO_x]$ is low and/or P_{HOx} is high) then $[HO_2 + RO_2]$ approaches $\sqrt{A}$ and is independent of $[NO_x]$. In contrast, when B is large relative to A ($[NO_x]$ is high and/or P_{HOx} is low) then $[HO_2 + RO_2]$ approaches zero. The lines in Figures 3b, 3d, and 3f are fits to the binned points that are obtained by minimizing the squares of the differences between the points and equation (11). The fit parameters are summarized in Table 4. It can be seen that the fits to the model data and to the measurements agree fairly well overall, but they are more consistent at low NO_x. This is because the concentrations tend to be larger, there tend to be more data per bin at low NO_x than at higher NO_x, and is possibly hinting at systematic differences between the model and measurements at high NO_x. Root mean square relative differences between the equation (9) fits to the measurements and the steady state model with and without C_2–C_4 carbonyl compounds, and the fit to the *Crawford et al.* [1999] model are 23, 7, and 7%, respectively, for NO_x from 10 to 1000 pptv and P_{HOx} from 0 to 0.3 pptv s^{-1}. Average ratios of these same three equation (11) fits to the Crawford et al. model fit are 0.76, 1.04, and 1.08, respectively.

[40] Root mean square differences between HO_2 fits for the measurements and the two steady state models and the Crawford HO_2 fit are 5, 8, and 8%, respectively (note that the fit to the measurements uses k_{RN} from the model fit). Average ratios of the HO_2 measurement and steady state model fits to the *Crawford et al.* [1999] model fit are 0.98, 1.07, and 1.06, respectively. Thus equation (9) describes the measurements and the various models well and may be a robust method of comparing and describing tropospheric peroxy radical levels. Application to other studies would further demonstrate its utility.

4.2. Radical Ratios

[41] Ratios of modeled or observed radical concentrations test our understanding of reactions that convert the radicals

Table 4. Parameters for Fits of Modeled and Measured Radical Levels and Ratios to Equation (11) ([HO_2 + RO_2] and [HO_2]), Equation (12) ([HO_2]/[OH]), Equation (13) ([HO_2 + RO_2]/[OH]), and Equation (14) ([HO_2 + RO_2]/[HO_2])[a]

Species or Ratio	Equation	Measured or Model	k_{RR}	k_{RN}			RMS Difference[b]
[HO_2 + RO_2]	11	C[c]	1.5×10^{-4}	0.9×10^{-5}			35%
[HO_2]	11	C	3.4×10^{-4}	1.0×10^{-5}			20%
[HO_2 + RO_2]	11	measured	1.8×10^{-4}	2.3×10^{-5}			61%
[HO_2]	11	measured	2.8×10^{-4}	1.0×10^{-5}[d]			76%
			X	y	w	z	
[HO_2]/[OH]	12	C	59	1.2	1.4	3.6×10^{-2}	22%
			a	b	c	d	
[HO_2 + RO_2]/[OH]	13	C	0.6	13	1.8×10^{-2}	5.7×10^{-4}	25%
			a	b	y	d	
[HO_2 + RO_2]/[HO_2]	14	C	1.2	7.6	2.7×10^{-2}	0.38	5%

[a]For these fits, P_{HOx} units are pptv s^{-1}, and the trace gas concentrations are pptv, except for CO which is ppbv.
[b]Relative percent root mean square difference between binned points and the fits.
[c]C designates use of model of *Crawford et al.* [1999], applied to TRACE-P conditions.
[d]There were not enough data points at high NO_x concentrations to constrain this parameter, so it was fixed to the model value.

between the various forms. For example, the ratio of HO_2 to OH has been shown to depend inversely on the NO concentration [e.g., *Brune et al.*, 1998; *Lanzendorf et al.*, 2001] and should also depend on the CO concentration since reactions involving NO and CO usually dominate in determining the radical ratio. Other species such as O_3, CH_2O, and H_2O_2 also contribute to radical conversion, and depending on the relative rates of the conversion reactions versus loss reactions, the latter may also affect HO_2/OH. Using modeled concentrations, a fit was performed to the following relationship:

$$\frac{[HO_2]}{[OH]} = \frac{x + y[CO]}{w + z[NO]}. \quad (12)$$

Here, *x* and *w* are represented as constant terms but encompass the contributions to this radical ratio from the processes involving species other than CO and NO; *y* and *z* are fit coefficients for the dependence of the ratio on CO and NO, respectively. The fit parameters are summarized in Table 4. Figure 9a shows the binned model data and fit lines, and Figure 9b shows binned measured ratios (based on these data and those of *Mauldin et al.* [2003]), colored by CO concentration and superimposed on the same model fit lines. The measured ratios are sufficiently noisy that fits are not significant. Figures 9a and 9b show that within the combined uncertainties of the measurements (about a factor of 2) there is approximate agreement between the modeled and observed ratios.

[42] The ratio of HO_2 + RO_2 to OH can be expressed in a manner similar to that for the HO_2 to OH ratio, as shown in equation (13).

$$\frac{[HO_2 + RO_2]}{[OH]} = \frac{a + b\sum(k_{OH}[RH])}{c + d[NO]}, \quad (13)$$

where *a* and *c* are constant terms that include the contribution due to reaction of OH with CO and other processes. The *b* coefficient represents the dependence of this radical ratio on the reaction of OH with methane and other hydrocarbons (the VOC reactivity, which ranges from about 0.05 to 1.6 s^{-1} for TRACE-P), and *d* represents the dependence on NO. The fit parameters derived from TRACE-P model results are shown in Table 4, and graphically in Figure 9c (colored by VOC reactivity). The fits to the model results are compared with measured radical ratios in Figure 9d.

[43] The ratio of HO_2 + RO_2 to HO_2 can be expressed using a similar simple equation.

$$\frac{[HO_2 + RO_2]}{[HO_2]} = a + \left(\frac{b\sum k_{OH}[RH]}{y[CO] + d[NO]}\right). \quad (14)$$

Parameters derived from fitting modeled HO_2 + RO_2 to HO_2 ratios are shown in Table 4. The fit is nearly as good eliminating the term containing CO. The bin averaged model results lead to [HO_2] fractions of [HO_2 + RO_2] ranging from 0.39 to 0.88 with most (90%) of the data falling between 0.62 and 0.88, larger values for lower hydrocarbon reactivity and a mean value of 0.75. PerCIMS measurements of HO_2 and HO_2 + RO_2 are not coincident, so ratios cannot be determined from individual observations. Measured data were binned in the same fashion as the model data (based on NO, CO and k_{OH}[RH]) and the ratios of the binned data lead to a mean value for [HO_2]/[HO_2 + RO_2] of 0.87 ($1\sigma = 0.44$). Given the uncertainties in the two independent measurements (about 35% for HO_2 + RO_2 and 50% for HO_2), this agrees well with the mean modeled ratio.

5. Photochemical Ozone Tendency

[44] Using observations and modeled quantities, we can estimate the in situ photochemical ozone production and destruction. Ozone is produced in the troposphere when peroxy radicals oxidize NO to NO_2 (reactions (13) and (14)) because it is the rate-limiting step in a sequence of reactions including the photolysis of NO_2 and oxidation of NO by O_3 and peroxy radicals. Ozone is destroyed by photolysis when the $O(^1D)$ product reacts with water vapor, and by reaction with OH and HO_2.

$$HO_2 + NO \rightarrow OH + NO_2 \quad (15)$$

$$RO_2 + NO(O_2) \rightarrow HO_2 + NO_2 + R'R''CO \quad (16)$$

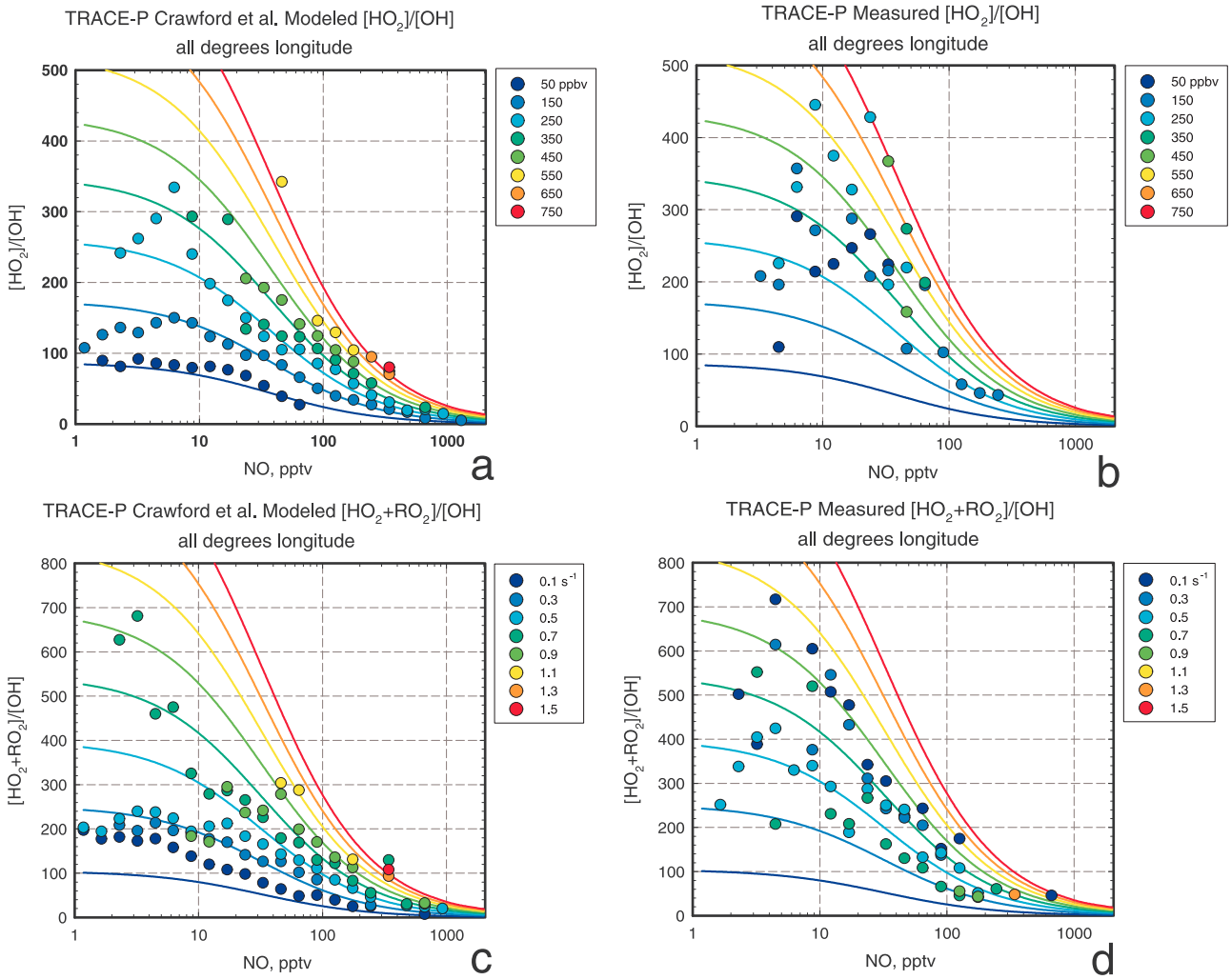

Figure 9. Radical ratios using (a and c) the *Crawford et al.* [1999] model results versus NO bin averages and (b and d) TRACE-P observations with points colored by CO (Figures 9a and 9b), and by VOC reactivity with OH (Figures 9c and 9d). Lines are fits to the model binned points using equations described in the text.

$$O_3 + h\nu \rightarrow O(^1D) + O_2$$

$$O(^1D) + H_2O \rightarrow 2\ OH$$

$$HO_2 + O_3 \rightarrow OH + 2O_2 \qquad (17)$$

$$OH + O_3 \rightarrow HO_2 + O_2. \qquad (18)$$

[45] The reaction of ozone with NO and the photolysis of NO_2 to produce NO and O_3 do not affect the net ozone tendency, although their occurrence is required for ozone production to take place. Since ozone is a secondary product of this chemistry (due to reactions (15) and (16)) and has additional sources such as transport from the stratosphere and elsewhere in the troposphere, its temporal and spatial distribution can be quite different from its source gases. The rates of ozone formation and destruction processes were calculated from TRACE-P observations and model results to produce a picture of ozone tendency during this campaign. Figure 10 shows several quantities relevant to ozone photochemistry. For these plots the data were binned by longitude, altitude, or NO concentration to produce about 20 to 100 bins. As mentioned earlier, most flights were during daylight hours with sampling approximately centered on local midday, regardless of longitude.

[46] In Figure 10a, several trace gas trends are shown versus the bin-averaged east longitude (degrees east of the Greenwich meridian). The longitude range covers the Pacific basin with eastern Asia to the west and western North America to the east. On average, the trace gases that are shown decrease markedly from the source region near Asia as the air masses are transported over the Pacific Ocean. The hydrocarbons are plotted as a corresponding amount of methane using the equivalent reactivity toward OH (VOC reactivity divided by k_{OH} for methane). Equivalent methane as used here corresponds to the OH reactivity of hydrocarbons expressed as an equal amount of methane. The net ozone tendency, N_{O3}, is defined as follows:

$$N_{O3} = P_{O3} - L_{O3}[O_3], \qquad (19)$$

where P_{O3} and L_{O3} are defined based on the following equations.

$$P_{O3} = [NO]\left(k_{13}[HO_2] + \sum k_{14,i}[RO_2]_i\right)$$

$$L_{O3} = j_1 Q + k_{15}[HO_2] + k_{16}[OH] \qquad (20)$$

$$Q = \frac{k_2[H_2O]}{k_{3a}[N_2] + k_{3b}[O_2] + k_2[H_2O]}$$

[47] The photolysis rate coefficient for ozone to $O(^1D)$ is represented by the *j*-value, and k_{3a} and k_{3b} are rate coefficients for quenching of $O(^1D)$ by nitrogen and oxygen, respectively (reaction (3)). The terms of the net ozone tendency are calculated using observed and modeled quantities. In the case of the peroxy radicals, two calculations were performed: one with observed HO_2 + RO_2 and one with peroxy radicals from the steady state model. Figure 10b shows bin averaged net ozone tendency versus longitude for these two cases. Error bars indicate the standard deviation of points within a bin and the absence of error bars indicates a bin with one or two points. It can be seen that west of 140° longitude, the average net O_3 tendency is always positive. Between 140° and 200° longitude, both positive and neg-

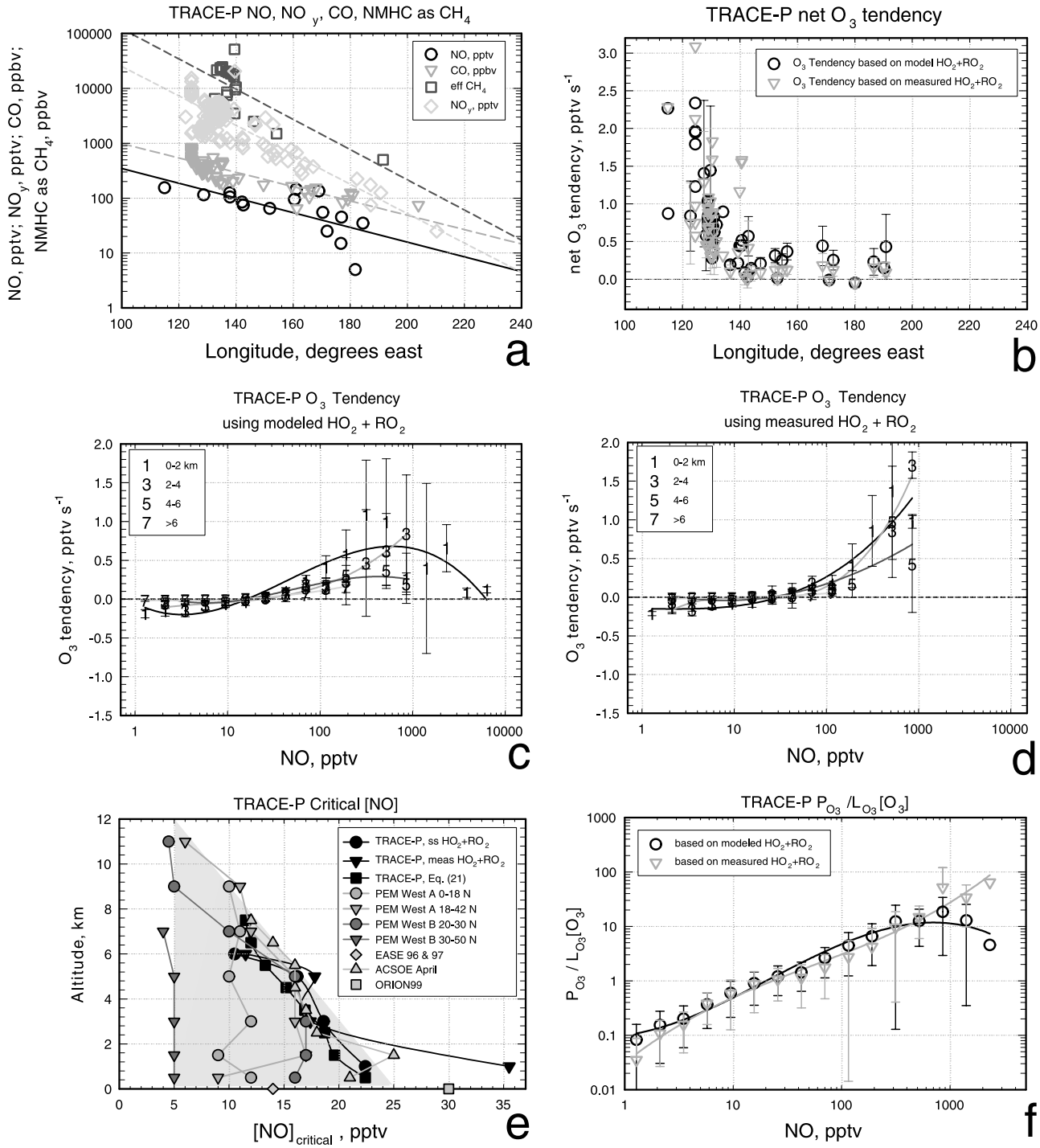

ative O_3 tendencies are observed, the magnitude of which depends somewhat on whether the measured or modeled peroxy radical concentrations are used. A clear relation is observed between the ozone tendency and the NO concentration as shown in Figures 10c and 10d. At average NO concentrations less than about 10–20 pptv, the tendency is always negative, while at larger NO concentrations the tendency is always positive, with a tendency for values at higher altitudes to be smaller than at lower altitudes. This critical NO, where the production and loss of ozone are in balance, has been discussed in the literature; some examples from PEM West A [*Davis et al.*, 1996], PEM West B [*Crawford et al.*, 1997], EASE [*Salisbury et al.*, 2002], ORION99 [*Kanaya et al.*, 2002] and ACSOE [*Reeves et al.*, 2002] are compared with those from TRACE-P in Figure 10e. Notice that the critical NO levels generally fill a triangular envelope bounded by about 5 pptv and a line between 25 pptv at the surface and 5 pptv at 12 km altitude (shown as gray shaded region in Figure 10e), although larger values in the boundary layer are observed (including calculations using peroxy radical measurements during TRACE-P). Location within the envelope depends on the importance of ozone photolysis as an ozone sink, the ozone and water concentrations, and the altitude. *Crawford et al.* [1997] present equations for production and loss of ozone, from which an equation can be derived that describes the critical NO as functions of these parameters. The results of this equation (also shown in Figure 10e) agree well with the TRACE-P observations.

$$[NO]_{critical} = \left(\frac{0.103}{2.19 \times 10^7}\right)[H_2O]^{0.1}\left(\frac{[O_3][M]\cos(\theta_{HN})}{TOMS}\right)^{0.5} \quad (21)$$

Here, [NO] is in pptv, $[H_2O]$ is in ppmv, $[O_3]$ is in ppbv, [M] is the air concentration in molecules cm^{-3}, θ_{HN} is the solar zenith angle of the sun at its highest (for the day and latitude), and TOMS is the overhead ozone column in Dobson units.

[48] The ratio of ozone production to loss ($P_{O3}/L_{O3}[O_3]$) is another quantity that is useful to describe the tendency. Values that are greater than unity describe air masses with positive tendency and those that are less than unity designate air masses with negative tendency. The relationships between this ratio and NO (Figure 10f) are very compact. There is a hint of reduction in this ratio for NO concentration bins larger than 1000 pptv using the modeled $HO_2 + RO_2$ (as expected since modeled peroxy radical concentrations decrease faster than NO_x increases in this concentration region) that is not evident in using the observed $HO_2 + RO_2$.

6. Summary

[49] Peroxy radicals, along with a number of trace gases, were measured aboard the P-3B aircraft during the TRACE-P mission. These data allow tests of our understanding of tropospheric chemistry. The functional dependence of peroxy radical levels on a number of controlling variables including the radical production rate and NO_x concentration appear to be robust and allow comparison of data from different observational studies. Recent rate coefficient and photolysis quantum yield reports lead to small changes in calculated peroxy radical concentrations. Suggestions that rate coefficients for reaction between HO_2 and RO_2 are smaller than recommended, based on a dependence of P_{HOx}/L_{HOx} on $F_{HO2+RO2}$, are not substantiated by this study.

[50] Comparison of measurements of peroxy radicals between two instruments on the two aircraft showed good agreement in one case and poorer agreement in another. Further comparisons between instruments from ground-based and aircraft platforms will help to understand these differences. The processes responsible for production of HO_x and RO_2 vary systematically with solar zenith angle and altitude in ways that can be understood by examination of the controlling variables. The ratio of $[HO_2 + RO_2]$ to the square root of P_{HOx} varies systematically with NO_x concentration. Peroxy radical concentrations appear to be reduced in the presence of aerosols and clouds as evidenced by systematic reduction in the measured to model ratio with increasing the aerosol surface area density or cloud liquid water content. Simple relations between trace gas concentrations and ratios of radical amounts are presented that may allow comparison between different studies but also could be used to calculate these quantities when direct observations are not available. Further tests are required to determine whether they hold universally or are only applicable to the conditions of TRACE-P. The observations of peroxy radicals and other trace gases can be used to estimate the photochemical ozone tendency, which was found to correlate strongly with NO and lead to net ozone production on average throughout the western Pacific basin. The central Pacific Ocean is a region of mixed ozone tendency probably depending on availability of reactive nitrogen transported from Asian urban regions and areas of biomass burning.

Figure 10. (opposite) (a) Bin-averaged trace gas concentrations versus longitude. (b) Bin-averaged net O_3 tendency (P_{O3}-$L_{O3}[O_3]$) versus longitude, with error bars showing the standard deviation of each bin. Average ozone tendency versus NO bin concentration using steady state modeled $HO_2 + RO_2$ (c) and measured $HO_2 + RO_2$ (d). Data points are labeled according to altitude, and error bars are the standard deviation of data within each sample bin. Lines are polynomial fits to the binned data. Critical NO values determined from x-axis crossovers of polynomial fits of the 5 or 6 values near zero O_3 tendency. (e) Critical NO concentrations (pptv) when O_3 tendency is zero ($P_{O3} = L_{O3}[O_3]$) as determined from measurements (black circles) and steady state model estimates (black triangles) of peroxy radicals during TRACE-P, using equation (21) derived from equations presented by *Crawford et al.* [1999] applied to TRACE-P conditions aboard the P-3B (black squares), and for a number of other observational studies (gray symbols): PEM West-A [*Davis et al.*, 1996], PEM West-B [*Crawford et al.*, 1999], EASE96 and 97 [*Salisbury et al.*, 2002], ACSOE [*Reeves et al.*, 2002], and ORION99 [*Kanaya et al.*, 2002]. Gray triangular area is a region that encompasses most of the observations. (f) Average ratio of ozone production (P_{O3}) to loss ($L_{O3}[O_3]$) versus NO bin concentration using steady state model $HO_2 + RO_2$ (circles) and measured $HO_2 + RO_2$ (triangles). Error bars represent the standard deviation of data within each bin.

[51] **Acknowledgments.** We thank the NASA TRACE-P Science Team for fruitful discussions and interchange during the field phase and in the data analysis part of this study. Also we are extremely grateful to the NASA project team including those responsible for standard measurements, preparation, and archiving of the data and care of the aircraft platforms. NCAR is sponsored by the National Science Foundation. This work was sponsored under NASA Research Cooperative Agreement NCC-1-424.

References

Apel, E. C., A. J. Hills, R. Lueb, S. Zindel, and S. Eisele, A fast-GC/MS system to measure C_2 to C_5 carbonyls and methanol aboard aircraft, *J. Geophys. Res.*, *108*(D20), 8794, doi:10.1029/2002JD003199, in press, 2003.

Brune, W. H., P. S. Stevens, and J. H. Mather, Measuring OH and HO_2 in the troposphere by laser-induced fluorescence at low pressure, *J. Atmos. Sci.*, *52*, 3328–3336, 1995.

Brune, W. H., et al., Airborne in situ OH and HO_3 observations in the cloud-free troposphere and lower stratosphere during SUCCESS, *Geophys. Res. Lett.*, *25*, 1701–1704, 1998.

Brune, W. H., et al., OH and HO_2 chemistry in the North Atlantic free troposphere, *Geophys. Res. Lett.*, *26*, 3077–3080, 1999.

Burkert, J., M. D. Andrés Hernández, D. Stöbener, and J. P. Burrows, Peroxy radical and related trace gas measurements in the boundary layer above the Atlantic Ocean, *J. Geophys. Res.*, *106*, 5457–5477, 2001.

Cantrell, C. A., R. E. Shetter, T. M. Gilpin, J. G. Calvert, F. L. Eisele, and D. J. Tanner, Peroxy radical concentrations measured and calculated from trace gas measurements in the Mauna Loa Observatory Photochemistry Experiment 2, *J. Geophys. Res.*, *101*, 14,653–14,664, 1996.

Cantrell, C. A., G. D. Edwards, S. Stephens, L. Mauldin, E. Kosciuch, M. Zondlo, and F. Eisele, Peroxy radical observations using chemical ionization mass spectrometry during TOPSE, *J. Geophys. Res.*, *108*(D6), 8381, doi:10.1029/2002JD002715, 2003a.

Cantrell, C. A., et al., Steady state free radical budgets and ozone photochemistry during TOPSE, *J. Geophys. Res.*, *108*(D4), 8361, doi:10.1029/2002JD002198, 2003b.

Christensen, L. E., M. Okumura, S. P. Sander, R. J. Salawitch, G. C. Toon, B. Sen, J. F. Blavier, and K. W. Jucks, Kinetics of $HO_2 + HO_2 \rightarrow H_2O_2 + O_2$: Implications for stratospheric H_2O_2, *Geophys. Res. Lett.*, *29*(9), 1299, 2002.

Clarke, A. D., Z. Li, and M. Litchy, Aerosol dynamics in the equatorial Pacific marine boundary layer: Microphysics, diurnal cycles and entrainment, *Geophys. Res. Lett.*, *23*(7), 733–736, 1996.

Crawford, J. H., et al., Implications of large scale shifts in tropospheric NO_x levels in the remote tropical Pacific, *J. Geophys. Res.*, *102*(D23), 28,447–28,468, 1997.

Crawford, J., et al., Assessment of upper tropospheric HOx sources over the tropical Pacific based on NASA GTE/PEM data: Net effect on HOx and other photochemical parameters, *J. Geophys. Res.*, *104*, 16,255–16,274, 1999.

Creasey, D. J., D. E. Heard, and J. D. Lee, OH and HO_2 measurements in a forested region of north-western Greece, *Atmos. Environ.*, *35*, 4713–4724, 2001.

Davis, D. D., Marine latitude/altitude OH distributions: Comparison of Pacific Ocean observations with models, *J. Geophys. Res.*, *106*(D21), 32,691–32,707, 2001.

Davis, D. D., et al., Assessment of ozone photochemistry in the western North Pacific as inferred from PEM-West A observations during the fall 1991, *J. Geophys. Res.*, *101*(D1), 2111–2134, 1996.

Edwards, G. D., C. A. Cantrell, S. Stephens, B. Hill, O. Goyea, R. E. Shetter, R. L. Mauldin III, E. Kosciuch, D. J. Tanner, and F. L. Eisele, Chemical ionization mass spectrometer instrument for the measurement of tropospheric HO_2 and RO_2, *Anal. Chem.*, in press, 2003.

Eisele, F. L., D. J. Tanner, C. A. Cantrell, and J. G. Calvert, Measurements and steady state calculations of OH concentrations at Mauna Loa Observatory, *J. Geophys. Res.*, *101*(D9), 14,665–14,679, 1996.

Eisele, F., et al., Summary of measurement intercomparisons during TRACE-P, *J. Geophys. Res.*, *108*(D20), 8791, doi:10.1029/2002JD003167, in press, 2003.

Elrod, M. J., D. L. Ranschaert, and N. J. Schneider, Direct kinetics study of the temperature dependence of the CH_2O branching channel for the $CH_3O_2 + HO_2$ reaction, *Int. J. Chem. Kinet.*, *33*, 363–376, 2001.

Faloona, I., et al., Observations of HO_x and its relationship with NO_x in the upper troposphere during SONEX, *J. Geophys. Res.*, *105*, 3771–3783, 2000.

Faloona, I., et al., Nighttime observations of anomalously high levels of hydroxyl radicals above a deciduous forest canopy, *J. Geophys. Res.*, *106*(D20), 24,315–24,333, 2001.

Hanson, D. R., J. B. Burkholder, C. J. Howard, and A. R. Ravishankara, Measurement of OH and HO_2 radical uptake coefficients on water and sulfuric acid surfaces, *J. Phys. Chem.*, *96*, 4979–4984, 1992.

Jacob, D. J., et al., Transport and chemical evolution over the Pacific (TRACE-P): A NASA/GTE aircraft mission, NASA, Washington, D. C., 1999. (Available at http://www-gte.larc.nasa.gov/trace/tracep.html)

Jacob, D. J., J. Crawford, M. M. Kleb, V. S. Connors, R. J. Bendura, J. L. Raper, G. W. Sachse, J. Gille, L. Emmons, and J. C. Heald, Transport and chemical evolution over the Pacific (TRACE-P) mission: Design, execution, and first results, *J. Geophys. Res.*, *108*(D20), 8781, doi:10.1029/2002JD003276, in press, 2003.

Jaeglé, L., et al., Photochemistry of HO_x in the upper troposphere at northern midlatitudes, *J. Geophys. Res.*, *105*(D3), 3877–3892, 2000.

Kanaya, Y., Y. Sadanaga, K. Nakamura, and H. Akimoto, Behavior of OH and HO_2 radicals during the Observations at a Remote Island of Okinawa (ORION99) field campaign: 1. Observation using a laser-induced fluorescence instrument, *J. Geophys. Res.*, *106*, 24,197–24,208, 2001.

Kanaya, Y., J. Matsumoto, and H. Akimoto, Photochemical ozone production at a subtropical island of Okinawa, Japan: Implications from simultaneous observations of HO_2 radical and NO_x, *J. Geophys. Res.*, *107*(D19), 4368, doi:10.1029/2001JD000858, 2002.

Lanzendorf, E. J., T. F. Hanisco, P. O. Wennberg, R. C. Cohen, R. M. Stimpfle, and J. G. Anderson, Comparing atmospheric $[HO_2]/[OH]$ to modeled $[HO_2]/[OH]$: Identifying discrepancies with reaction rates, *Geophys. Res. Lett.*, *28*(6), 967–970, 2001.

Mauldin, R. L., III, et al., Highlights of OH, H_2SO_4, and MSA measurements made aboard the NASA P-3B during TRACE-P, *J. Geophys. Res.*, *108*(D20), 8796, doi:10.1029/2003JD003410, in press, 2003.

Mozurkewich, M., P. H. Murry, A. Gupta, and J. G. Calvert, Mass accommodation coefficient for HO2 radicals on aqueous particles, *J. Geophys. Res.*, *92*, 4163–4170, 1987.

Olson, J. R., et al., Seasonal differences in the photochemistry of the South Pacific: A comparison of observations and model results from PEM-Tropics A and B, *J. Geophys. Res.*, *106*, 32,749–32,766, 2001.

Ravishankara, A. R., E. J. Dunlea, M. A. Blitz, T. J. Dillon, D. E. Heard, M. J. Pilling, R. S. Strekowski, J. M. Nicovich, and P. H. Wine, Redetermination of the rate coefficient for the reaction of $O(^1D)$ with N_2, *Geophys. Res. Lett.*, *29*(15), 1745, doi:10.1029/2001GL014850, 2002.

Reeves, C. E., et al., Potential for photochemical ozone formation in the troposphere over the North Atlantic as derived from aircraft observations during ACSOE, *J. Geophys. Res.*, *107*(D23), 4707, doi:10.1029/2002JD002415, 2002.

Salisbury, G., P. S. Monks, S. Bauguitte, B. J. Bandy, and S. A. Penkett, A seasonal comparison of the ozone photochemistry in clean and polluted air masses at Mace Head, Ireland, *J. Atmos. Chem.*, *41*, 163–187, 2002.

Sander, S. P., et al., Chemical kinetics and photochemical data for use in atmospheric studies, evaluation number 14, *JPL Publ. 02–25*, Jet Propul. Lab., Pasadena, Calif., 2002. (Available at http://jpldataeval.jpl.nasa.gov)

Saylor, R., An estimate of the potential significance of heterogeneous loss to aerosols as an additional sink for hydroperoxy radicals in the troposphere, *Atmos. Environ.*, *31*, 3653–3658, 1997.

Schwartz, S. E., Gas and aqueous-phase chemistry of HO_2 in liquid water clouds, *J. Geophys. Res.*, *89*, 11,589–11,598, 1984.

Sillman, S., et al., Loss of isoprene and sources of OH radicals at a rural site in the United States: Results from photochemical models, *J. Geophys. Res.*, *107*(D5), 4043, doi:10.1029/2001JD000449, 2002.

Singh, H. B., et al., In situ measurements of HCN and CH_3CN over the Pacific Ocean: Sources, sinks, and budgets, *J. Geophys. Res.*, *108*(D20), 8795, doi:10.1029/2002JD003006, in press, 2003.

Smith, G. D., L. T. Molina, and M. J. Molina, Measurement of radical quantum yields from formaldehyde photolysis between 269 and 339 nm, *J. Phys. Chem. Ser. A*, *106*(7), 1233–1240, 2002.

Stevens, P. S., et al., HO_2/OH and RO_2/HO_2 ratios during the Tropospheric OH Photochemistry Experiment: Measurement and theory, *J. Geophys. Res.*, *102*, 6379–6391, 1997.

Swietlicki, E., et al., Hygroscopic properties of aerosol particles in the north-eastern Atlantic during ACE-2, *Tellus, Ser. B*, *32*, 102–227, 2000.

Tan, D., et al., OH and HO_2 in the tropical Pacific: Results from PEM-Tropics B, *J. Geophys. Res.*, *106*, 32,667–32,681, 2001.

Thornton, J. A., et al., Ozone production rates as a function of NO_x abundances and HO_x production rates in the Nashville urban plume, *J. Geophys. Res.*, *107*(D12), 4146, doi:10.1029/2001JD000932, 2002.

Walcek, C. J., H.-H. Yuan, and W. R. Stockwell, The influence of aqueous phase chemical reactions on ozone formation in polluted and nonpolluted clouds, *Atmos. Environ.*, *31*, 1221–1237, 1997.

Wennberg, P. O., et al., Hydrogen radicals, nitrogen radicals, and the production of O_3 in the upper troposphere, *Science*, *279*, 49–53, 1998.

Zanis, P., P. S. Monks, E. Schuepbach, and S. A. Penkett, On the relationship of $HO_2 + RO_2$ with $j(O^1D)$ during the Free Tropospheric Experiment

(FREETEX '96) at the Jungfraujoch Observatory (3580 m above sea level) in the Swiss Alps, *J. Geophys. Res.*, *104*, 26,913–26,925, 1999.

E. Apel, C. A. Cantrell, F. L. Eisele, F. Flocke, A. Fried, S. Hall, E. Kosciuch, B. L. Lefer, R. L. Mauldin, R. E. Shetter, S. Stephens, and A. Weinheimer, Atmospheric Chemistry Division, National Center for Atmospheric Research, Boulder, CO 80305, USA. (apel@ucar.edu; cantrell@ucar.edu; eisele@ucar.edu; ffl@ucar.edu; fried@ucar.edu;halls@ucar.edu; kosciuch@ucar.edu; lefer@ucar.edu; maudlin@ucar.edu; shetter@ucar.edu; steph@ucar.edu; wein@ucar.edu)

M. A. Avery, J. D. Barrick, J. H. Crawford, J. R. Olson, and G. W. Sachse, NASA Langley Research Center, Hampton, VA 23681, USA. (m.a.avery@larc.nasa.gov; j.d.barrick@larc.nasa.gov; j.h.crawford@larc.nasa.gov; j.r.olson@larc.nasa.gov; g.w.sachse@larc.nasa.gov)

A. R. Bandy and D. C. Thornton, Drexel University, Philadelphia, PA 19104, USA. (bandyar@drexel.edu; dct@drexel.edu)

D. R. Blake, N. J. Blake, and I. J. Simpson, University of California, Irvine, Irvine, CA 92697, USA. (drblake@uci.edu; nblake@uci.edu; isimpson@uci.edu)

W. H. Brune, Pennsylvania State University, University Park, PA 16802, USA. (whb2@psu.edu)

A. D. Clarke, School of Oceanography and SOEST, University of Hawaii at Manoa, Honolulu, HI 96822, USA. (tclarke@soest.hawaii.edu)

G. D. Edwards, Department of Chemistry, Purdue University, West Lafayette, IN 47907, USA. (gdedward@perdue.edu)

H. Harder and M. Martinez, Max Planck Institute for Chemistry, 55128 Mainz, Germany. (harder@mpch-mainz.mpg.de; martinez@mpch-mainz.mpg.de)

B. G. Heikes, University of Rhode Island, Narragansett, RI 02881, USA. (zagar@notos.gso.uri.edu)

D. J. Jacob, Harvard University, Cambridge, MA 02138, USA. (djj@io.harvard.edu)

Y. Kondo, Research Center for Advanced Science and Technology, University of Tokyo, Tokyo, Japan 153-8904. (kondo@atmos.rcast.u-tokyo.ac.jp)

H. B. Singh, NASA Ames Research Center, Moffett Field, CA 94035, USA. (hsingh@mail.arc.nasa.gov)

M. A. Zondlo, Southwest Sciences Inc., Santa Fe, NM 87505, USA. (mzondlo@swisciences.com)